Systematic identification of host cell regulators of *Legionella pneumophila* pathogenesis using a genome-wide CRISPR screen

Edwin E. Jeng[1,2], Varun Bhadkamkar[3], Nnejiuwa U. Ibe[3], Haley Gause[3], Lihua Jiang[1], Joanne Chan[1], Ruiqi Jian[1], David Jimenez-Morales[4,5], Erica Stevenson[4], Nevan J. Krogan[4], Danielle L. Swaney[4], Michael P. Snyder[1], Shaeri Mukherjee[3,*], Michael C. Bassik[1,6,*]

[1]Department of Genetics, Stanford University School of Medicine, Stanford, CA 94305, USA

[2]Program in Cancer Biology, Stanford University School of Medicine, Stanford, CA 94305, USA

[3]Department of Microbiology and Immunology, University of California, San Francisco, San Francisco, CA 94143, USA

[4]Department of Cellular and Molecular Pharmacology, University of California San Francisco, San Francisco, CA, USA; Quantitative Biosciences Institute (QBI), University of California San Francisco, San Francisco, CA, USA; The J. David Gladstone Institutes, San Francisco, CA, USA

[5]Current address: Department of Medicine, Division of Cardiovascular Medicine. Stanford University, Stanford, CA 94305

[6]Lead Contact

Summary:

During infection, *Legionella pneumophila* translocates over 300 effector proteins into the host cytosol, allowing the pathogen to establish an endoplasmic reticulum (ER)-like *Legionella*-containing vacuole (LCV) that supports bacterial replication. Here, we perform a genome-wide CRISPR-Cas9 screen and secondary targeted screens in U937 human monocyte/macrophage-like cells to systematically identify host factors that regulate killing by *L. pneumophila*. The screens reveal known host factors hijacked by *L. pneumophila* as well as genes spanning diverse trafficking and signaling pathways previously not linked to *L. pneumophila* pathogenesis. We further characterize *C1orf43* and *KIAA1109* as regulators of phagocytosis, and show that *RAB10* and its chaperone *RABIF* are required for *L. pneumophila* replication and ER recruitment to the

LCV. Finally, we show that Rab10 protein is recruited to the LCV and ubiquitinated by the effectors SidC/SdcA. Collectively, our results provide a wealth of previously undescribed insights into *L. pneumophila* pathogenesis and mammalian cell function.

Graphical Abstract:
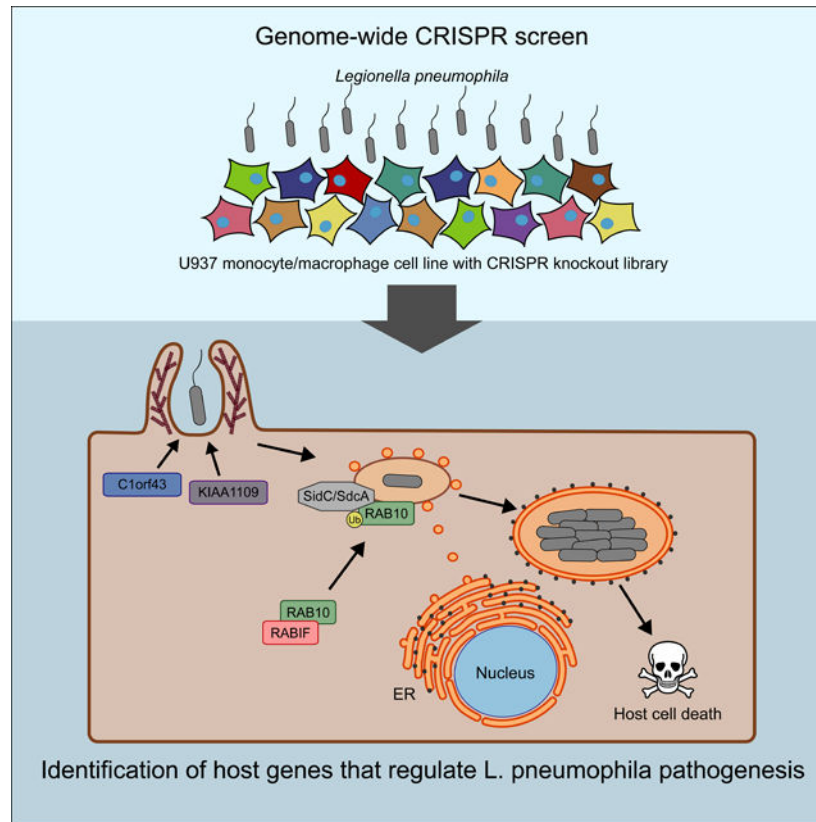
eTOC:

Jeng et al. perform a genome-wide CRISPR knockout screen to systematically identify host factors that regulate killing by *Legionella pneumophila*. The screen identifies hundreds of known and unknown factors. Among these, the authors further characterize regulators of phagocytosis, intracellular bacterial replication, and formation of the *Legionella*-containing vacuole (LCV).

Introduction:

Legionella pneumophila is a gram-negative intracellular bacterial pathogen, and the causative agent of a severe form of pneumonia called Legionnaires' disease (Horwitz and Silverstein, 1980; Rowbotham, 1980). Following phagocytosis by alveolar macrophages, *L. pneumophila* translocates over 300 effector proteins into the host cytosol through a type IV secretion system called Dot/Icm to alter numerous host pathways, including membrane trafficking (Ninio and Roy, 2007), apoptosis (Banga et al., 2007), and ER stress (Treacy-Abarca and Mukherjee, 2015), and promote its own survival and replication. A hallmark of

L. pneumophila infection is its ability to avoid lysosomal degradation, instead forming an ER-like LCV permissive for replication (Horwitz, 1983a, b).

Because it can manipulate multiple host processes, *L. pneumophila* has become a major discovery tool to not only study aspects of pathogenesis, but also to shed light on host cell biology. For example, previous studies on *L. pneumophila* have uncovered a novel post-translational modification (phosphocholination) (Mukherjee et al., 2011), an unusual form of ubiquitination that is not dependent on E1 and E2 enzymes (Bhogaraju et al., 2016; Qiu et al., 2016), as well as a unique mechanism to inhibit autophagy by deconjugating Atg8/LC3 proteins coupled to phosphatidylethanolamine on autophagosomal membranes (Choy et al., 2012), to name a few. Given the vast repertoire of effectors secreted by *L. pneumophila* and numerous host processes targeted, it is not surprising that there are still major unsolved questions. Despite breakthroughs to understand the functions of some effectors, our knowledge of *L. pneumophila*-host interactions on a genomic scale remains fairly limited. One major obstacle is that single genetic deletions of *L. pneumophila* effectors rarely display a phenotype, likely due to effector redundancy (Luo and Isberg, 2004; O'Connor et al., 2011; Ragaz et al., 2008). As a result, the field has predominantly relied on biochemical studies of effectors to identify their function and host targets.

An alternative approach to studying *L. pneumophila* host-pathogen interactions is focusing on host factors. RNA interference (RNAi) screens in *Drosophila melanogaster* S2 cells covering around half the *Drosophila* genome have helped identify host processes that regulate *L. pneumophila* replication, including genes involved in vesicle trafficking, ER-associated degradation, protein translation, and cell cycle progression (de Jesus-Diaz et al., 2017; Dorer et al., 2006). Yet these screens identified relatively few host factors that displayed *L. pneumophila* replication defects from single gene knockdowns; instead, silencing multiple genes was frequently required. Whether this is due to incomplete inhibition of host factors via RNAi or differences between *Drosophila* S2 cells and mammalian macrophages (a more natural target cell for *L. pneumophila*) is unclear. At the same time, a systematic study of the impact of host factors on *L. pneumophila* infection has not been conducted in mammalian cells. With the development of improved strategies for pooled CRISPR-Cas9 deletion screens (Adamson et al., 2016; Haney et al., 2018; Koike-Yusa et al., 2014; Morgens et al., 2017; Parnas et al., 2015; Shalem et al., 2014; Wang et al., 2014; Zhou et al., 2014), robust genome-wide gene deletion screens in most commonly used mammalian cell models are now possible.

Here, we perform a genome-wide CRISPR screen and targeted follow-up screens to systematically identify hundreds of human host factors that suppress or enhance *L. pneumophila* killing of U937 monocyte/macrophage cells, which span diverse known and yet undescribed pathways. We define roles for two previously uncharacterized genes (*C1orf43* and *KIAA1109*) in regulating phagocytosis, and identify a requirement for *RAB10* and the chaperone *RABIF* in *L. pneumophila* replication and LCV maturation. We further explore how Rab10 is hijacked by *L. pneumophila* during infection: it is recruited to the LCV and also ubiquitinated by the effectors SidC and SdcA. Together, these results illuminate new factors that control trafficking, and represent a powerful resource for

advancing our understanding of how host macrophages interact with *L. pneumophila* during infection.

Results:

Genome-wide CRISPR-Cas9 screen for host cell regulators of *L. pneumophila* pathogenesis

To identify host cell genes that control *L. pneumophila* pathogenesis, we performed a genome-wide CRISPR-Cas9 knockout screen in the human monocytic cell line, U937. Wild-type (WT) *L. pneumophila* can readily infect, replicate intracellularly, and kill this cell line while an isogenic, nonpathogenic *dotA* strain incapable of secreting effectors into the host cytosol is efficiently cleared by the host (Fig. 1A) (Berger et al., 1994). First, we infected Cas9-expressing U937 cells with a lentiviral sgRNA library consisting of ten single-guide RNAs (sgRNAs) per gene targeting ~20,500 human genes as well as ~10,000 negative control sgRNAs (Morgens et al., 2017) (Fig. 1B). Then, we split the cells into two populations – one was infected with *L. pneumophila* at a multiplicity of infection (MOI) of 100 while the other remained uninfected over the duration of the screen. We added the antibiotic rifampicin, which does not affect the growth of U937 cells (Fig. S1A), 24 hours post-infection (hpi) to kill off all bacteria and allowed the cells to recover. We repeated this cycle a total of five times to increase selection (Fig. S1B) and then used deep sequencing to quantify the effect of each sgRNA between the *L. pneumophila*-infected and uninfected populations. sgRNAs causing gene deletions that protected cells from *L. pneumophila* toxicity were enriched, whereas those that sensitized cells were depleted in the population. To determine gene-level phenotypes, we used the Cas9 high-throughput maximum-likelihood estimator (casTLE) algorithm (Morgens et al., 2016) (see Methods for additional details). Top hits showed strong enrichment or depletion across multiple sgRNAs compared to the population of negative controls (Fig. S1C).

The screen identified 186 genes that suppressed or enhanced *L. pneumophila* killing at a 10% false discovery rate (FDR) (Fig. 1C, Table S1). Our approach effectively captured biologically meaningful regulators of *L. pneumophila* pathogenesis, as several positive controls were identified as protective hits at FDR 10%, including actin regulators necessary for phagocytosis (RAC1, ARP2/3 complex, and SCAR/WAVE complex) (Haney et al., 2018; Mao and Finnemann, 2015; May et al., 2000) as well as *RAB1A*, a key GTPase hijacked by *L. pneumophila* for ER recruitment during LCV formation (Derre and Isberg, 2004; Ingmundson et al., 2007; Kagan et al., 2004). Notably, enrichment analysis for Gene Ontology (GO) terms highlighted a number of pathways not previously linked to *L. pneumophila* biology such as peroxisomal protein import and the vesicle trafficking adaptor AP-3 complex, in addition to expected pathways (e.g. phagocytosis, actin regulation, ER-to-Golgi vesicle trafficking) (Hubber and Roy, 2010) (Fig. 1D).

Batch retest screens and competitive killing assays validate host regulators of *L. pneumophila* pathogenesis

We next performed a smaller-scale "batch retest" screen at higher coverage (4000 vs. 1000 cells per sgRNA), which we and others have shown can reduce false positives and false

negatives (Bassik et al., 2013; Han et al., 2017; Haney et al., 2018; Parnas et al., 2015). For this custom library, we included 1139 genes consisting of the 186 genes that were hits in the genome-wide screen at 10% FDR, factors previously identified in LCVs isolated from macrophages (Hoffmann et al., 2014), and additional genes of interest, such as genes involved in trafficking (Fig. 1E, Table S2). The batch retest screen showed strong correlation between replicates (Fig. S1D) and moderate correlation with the genome-wide screen (Fig. 1F), and revealed additional hits that were not significant in the genome-wide screen (Fig. S1E, Fig. 1F). Of note, of 19 additional genes that were hits with a less stringent 20% FDR cutoff in the genome-wide screen and included in the batch retest library, 18 were hits in the batch retest screen (Table S3). These results suggest that genes that fell outside of the 10% FDR cutoff in the genome-wide screen can still be meaningful hits.

Overall, the screens revealed a comprehensive picture of host pathways involved in *L. pneumophila* pathogenesis (Fig. 2A, Table S3). As in the genome-wide screen, the protective effect of deleting actin-regulating genes (ARP2/3 complex, SCAR/WAVE complex, Rac signaling, actin cytoskeleton) represented one of the strongest signatures. We and others have previously shown that many of these genes are necessary for phagocytosis (Haney et al., 2018; Mao and Finnemann, 2015; May et al., 2000; Philips et al., 2005; Zhang et al., 1998), which is the natural mechanism by which *L. pneumophila* enters host cells (Hubber and Roy, 2010). Because manipulation of ER-to-Golgi transport machinery to recruit ER-derived vesicles to the LCV is a hallmark of *L. pneumophila* pathogenesis (Hubber and Roy, 2010), we expected to find many of these components among the protective hits. Indeed, deletion of the GTPases *RAB1A* and *ARF1*, whose activities are directly hijacked by *L. pneumophila* effectors and are required for LCV formation, protected cells *from L. pneumophila* killing (Derre and Isberg, 2004; Ingmundson et al., 2007; Kagan and Roy, 2002; Kagan et al., 2004), along with genes spanning multiple steps of the ER-to-Golgi trafficking pathway including COPII vesicle biogenesis (*SAR1A*, *SEC13*, *SEC23B*) and most members of all three known mammalian TRAPP complexes. Orthologs of *TRAPPC1* and *TRAPPC3* were previously shown in *Drosophila* S2 cells to impair *L. pneumophila* replication when depleted in combination with other secretory pathway genes (Dorer et al., 2006). Many additional ER- and Golgi-resident genes were identified as strong regulators of *L. pneumophila* pathogenesis and may play roles in LCV formation and maturation into an ER-like vacuole. Outside of the ER and Golgi, the screen revealed a protective effect for deletion of 7 members of the exocyst complex (*EXOC1-3*, *EXOC5-8*) and logically consistent effects for both positive (*RAB10*, *RALGDS*) and negative (*RALGAPA1*, *RALGAPB*) regulators of exocyst assembly. Recently, members of the exocyst complex (*EXOC2* and *EXOC6*), normally involved in post-Golgi trafficking, were shown to tether ER-derived vesicles to the LCV in a DrrA-dependent manner (Arasaki et al., 2018). Additionally, the plasma membrane-localized SNARE protein SNAP23 was found to bind Sec22b and localize to the LCV during *L. pneumophila* infection (Arasaki and Roy, 2010).

Intriguingly, we also identified multiple members of complexes and pathways that have not been previously linked to *L. pneumophila* pathogenesis: deletion of peroxisome protein import genes (*PEX5*, *PEX10*, *PEX12*) was protective while deletion of genes in clathrin-coated vesicle assembly (*CLTC*, *PICALM*, *SH3GL1*), the ESCRT-III complex (*CHMP2A*,

CHMP6), and the AP-3 complex (*AP3B1, AP3D1*) was sensitizing. These results implicate a number of additional processes as regulators of *L. pneumophila* pathogenesis.

We next validated a panel of hits from the batch retest screen with individual sgRNAs in an orthogonal competitive killing assay, in which we mixed GFP-positive knockout cells with mCherry-positive negative control cells and measured the relative enrichment or depletion of the GFP-positive cells after *L. pneumophila* infection compared to an uninfected control. We tested 15 genes with two top-performing sgRNAs and all validated in these assays, confirming the screen results (Fig. 2B). Gene deletion was confirmed for selected sgRNAs by indel analysis using TIDE (Brinkman et al., 2014) (Fig. S2A).

To determine whether the identified regulators are important for controlling *L. pneumophila* pathogenesis in more macrophage-like cells, we performed an additional screen in phorbol 12-myristate 13-acetate (PMA)-differentiated U937 cells (Koeffler, 1983) using the same batch retest library. Because PMA treatment of U937 cells causes the cells to become non-proliferative, we maximized the dynamic range for the single pulse screen by plating differentiated U937 cells containing the sgRNA library at 8000 cells per sgRNA and infecting the cells with *L. pneumophila* at MOI = 60, which was sufficient to kill ~80% of the cells (Fig. S2B). As before, the surviving cells were collected and sgRNA abundances were compared to an uninfected but differentiated control population by deep sequencing. Although the screen in differentiated U937 cells had smaller effect sizes and was less reproducible due to the single round of infection (Figs. S2C, S2D), many hits including actin regulators, uncharacterized genes *C1orf43* and *KIAA1109*, and various trafficking genes (e.g. *RAB1A*, *ARF1*, *SNAP23*, TRAPP complex members, and *RABIF*) remained strong and reproducible hits (Fig. S2E, Table S3).

Interestingly, certain genes appeared to have effects that were cell-state specific; for example, knockout of exocyst components had little effect on *L. pneumophila* pathogenesis in differentiated U937 cells while deletion of HOPS complex members predominantly reduced pathogenesis in differentiated cells (Fig. S2E). Differences between the two screens might be attributed to many factors, including weaker selection in differentiated cells, gene expression differences, or differential requirements for bacterial replication in monocyte vs. macrophage cells. Altogether, the combination of an unbiased genome-wide screen and secondary targeted screens in two cell states identified many known and additional processes that control *L. pneumophila* pathogenesis.

C1orf43 and *KIAA1109* are regulators of phagocytosis

Since the screens identified host factors that could act at multiple stages of the *L. pneumophila* infection cycle, e.g. uptake, LCV maturation, and replication, we next sought to define which step of infection selected hits are involved in. We selected 9 genes that protected host cells from *L. pneumophila* pathogenesis in both differentiated and undifferentiated batch retest screens for further exploration, including positive controls, uncharacterized genes, and membrane trafficking genes whose roles in *L. pneumophila* biology are not understood. We tested if these genes regulate phagocytosis of pHrodo dye-conjugated nonpathogenic *dotA L. pneumophila*. Here, delivery of bacteria to the low pH

environment of late endosomes and lysosomes after uptake can be measured by automated fluorescence microscopy (Fig. S3A).

Most tested hits such as *RABIF*, *RAB10*, and *C10orf76* were protective against killing but did not affect phagocytosis, (Fig. 3A), suggesting that these genes play a downstream role in the intracellular replication of *L. pneumophila* (see below). In contrast, knockouts of the uncharacterized genes *C1orf43* and *KIAA1109* significantly impaired phagocytosis of *L. pneumophila* with two independent sgRNAs (Fig. 3A), as did a positive control gene *ABI1*, which is a component of the SCAR/WAVE complex that controls actin polymerization of the phagocytic cup (Rougerie et al., 2013). KIAA1109 is a large, 5,005 amino acid protein with no known domains or motifs. Mutants of the *Drosophila* ortholog *tweek* have reduced phosphatidylinositol-4,5-bisphosphate [$PI(4,5)P_2$] at synapses, resulting in decreased Wiscott-Aldrich syndrome protein (WASP)-dependent actin polymerization and decreased synaptic vesicle recycling (Khuong et al., 2010; Verstreken et al., 2009). Recently, similar defects in endosomal recycling and changes in the actin cytoskeleton were shown in human primary fibroblasts from patients with biallelic variants in *KIAA1109* (Kane et al., 2019). Because endocytic membrane recycling (Cox et al., 2000) and $PI(4,5)P_2$ accumulation at the phagocytic cup (Botelho et al., 2000) are both required for efficient phagocytosis, it is possible that KIAA1109 plays a similar role in regulating these processes in macrophages during phagocytosis.

We chose to further investigate the role of C1orf43, a ubiquitously expressed, 253 amino acid protein as it has no known function and is conserved from *Drosophila* to humans. To determine whether *C1orf43* plays a general role in phagocytosis or specifically in *L. pneumophila* uptake, we tested the ability of U937 *C1orf43* clonal knockouts (Fig. S3B) to phagocytose various pHrodo-labeled substrates (Figs. 3B, C). *C1orf43* knockout cells had a strong defect in the uptake *L. pneumophila* and another gram-negative bacterium *Escherichia coli*, gram-positive *Staphylococcus aureus*, zymosan (made from yeast cell wall), and 1 μm polystyrene beads. Importantly, phagocytosis of these diverse substrates by U937 cells is dependent on actin dynamics and blocked by cytochalasin D. The phagocytosis defect was additionally observed in Raw 264.7 mouse macrophages when the *C1orf43* mouse ortholog *4933434E20Rik* was deleted (Fig. 3D). These results are consistent with a role for C1orf43 as a general regulator of phagocytosis.

Expression of a full-length FLAG-tagged C1orf43, but not its N-terminal single-pass transmembrane domain (C1orf43$_{1-41}$), re-sensitized *C1orf43* knockout cells to killing by *L. pneumophila* (Figs. 3E, S3C). This suggests the intracellular C-terminal region of *C1orf43* is necessary for its activity. Of note, expression of a C1orf43 isoform lacking the transmembrane domain (C1orf43 $_{TM}$) could not be detected by immunoblot, likely due to protein instability (Fig. S3C).

To further characterize C1orf43, we examined the localization of a C1orf43 C-terminal GFP fusion protein in HeLa cells. Expression of C1orf43-GFP localized predominantly to the Golgi, with weaker staining in the mitochondria (Fig. S3D). C1orf43-GFP remained stably co-localized with Golgi markers even following treatment with two compounds, Brefeldin A and nocodazole, that disrupt the Golgi via distinct mechanisms (Fig. S3E). Furthermore, we

did not observe changes in C1orf43-GFP localization during *L. pneumophila* infection (Fig. S3F, Video S1).

Next, we examined protein interactors of C1orf43 that were identified in the BioPlex database, which contains almost 6000 affinity purification mass spectrometry (AP-MS) experiments performed in HEK293T cells (Huttlin et al., 2017). In this dataset, C1orf43 was shown to interact with 24 other proteins (Fig. S3G). GO term analysis revealed strong enrichment of plasma membrane proteins, with over half of the identified proteins annotated as integral components of the plasma membrane, including ion channels and transporters as well as cell adhesion molecules (Fig. S3H).

Together, these data demonstrate that C1orf43 is required for phagocytosis of diverse particles. Given the variable localization and protein interactors suggested by our studies and publicly available data, further investigation will be required to fully define its mechanism of action.

RABIF regulates *L. pneumophila* replication and ER recruitment to the LCV by stabilizing Rab10 expression

We next examined whether our selected hits are involved in intracellular replication of mCherry-expressing *L. pneumophila* using automated fluorescence microscopy (Fig. S4A), with mCherry intensity as a readout of *L. pneumophila* burden (Fig. S4B). As expected, gene knockouts that protected host cells against *L. pneumophila* killing also resulted in significantly decreased *L. pneumophila* burden in undifferentiated U937 cells (Fig. S4C). Furthermore, gene knockouts other than the exocyst complex members *EXOC7* and *EXOC8* also had a reduced *L. pneumophila* burden when tested in differentiated U937 macrophage-like cells (Fig. 4A). A reduced *L. pneumophila* burden can reflect defects in both *L. pneumophila* uptake and intracellular replication. Therefore, since knockouts of genes such as *RABIF*, *RAB10*, and *C10orf76* result in reduced *L. pneumophila* burden but did not affect uptake (Figs. 4A, 3A), these genes likely play a downstream role in intracellular replication of *L. pneumophila* after the bacterium is phagocytosed. The replication defect was even more pronounced in clonal knockouts of *RABIF* and *RAB10* (Figs. 4B, S4D).

Because *RABIF* was also one of the strongest hits in both undifferentiated and differentiated U937 batch retest screens (Fig. S2E) we sought to determine the mechanism by which *RABIF* regulates *L. pneumophila* replication. We performed APMS using GFP-RABIF as a bait protein expressed in U937 cells to identify RABIF interactors. We found that RABIF co-immunoprecipitated a number of Rabs, including Rab1a, Rab1b, Rab8a, Rab8b, Rab10, Rab13, and Rab35 (Fig. 4C, Table S4), consistent with previous reports (Gulbranson et al., 2017; Wixler et al., 2011).

Interestingly, only knockouts of *RAB1A* and *RAB10* were protective against *L. pneumophila* pathogenesis in the screen (Figs. 1C, 2A), and RABIF has been shown to stabilize a subset of Rabs (Gulbranson et al., 2017). We therefore tested whether RABIF had a direct effect on protein levels of Rab1a and Rab10, which could explain the protective effect of *RABIF* knockout. Indeed, *RABIF* knockout resulted in a near complete loss of Rab10 protein, while Rab1a levels remained unchanged (Fig. 4D). Given the similar *L.*

pneumophila replication defect in *RABIF* and *RAB10* knockout cells (Fig. 4B) and the regulation of Rab10 protein levels by RABIF, RABIF is likely acting through Rab10 during *L. pneumophila* infection.

Since remodeling of the LCV into an ER-like vacuole is a critical step in creating a permissive environment for *L. pneumophila* replication (Hubber and Roy, 2010), we investigated whether *RABIF* and *RAB10* regulate ER recruitment to the LCV. Here, we used HeLa cells stably expressing the FcγRII receptor (HeLa FcγRII), which allows efficient internalization of opsonized *L. pneumophila* into non-phagocytic cells (Mukherjee et al., 2011). Knockout of *RABIF* and *RAB10* in HeLa FcγRII cells significantly impaired co-localization of the resident ER protein Reticulon 4 (RTN4) with the LCV at 4 hpi (Figs. 4E, F). Furthermore, expression of a dominant negative GDP-locked form of Rab10 (Rab10 T23N) but not a GTP-locked form (Rab10 Q68L) (Babbey et al., 2006) decreased RTN4 recruitment to the LCV compared to cells expressing WT Rab10, suggesting Rab10 activity plays a role in remodeling the LCV into an ER-like vacuole (Fig. S5A). Because a decrease in RTN4 recruitment could be confounded by increased phagosome-lysosome fusion, we also examined whether *RABIF* and *RAB10* knockout affects LAMP1 acquisition on the LCV. *RABIF* and *RAB10* knockout had no significant effect on LAMP1 acquisition, supporting their roles in ER recruitment to the LCV (Fig. S5B, C). The role of RABIF stabilization of Rab10 highlights Rab10 as a key host protein for *L. pneumophila* replication and ER recruitment to the LCV. We thus sought to further characterize how *L. pneumophila* hijacks Rab10 during infection.

Rab10 is recruited to the LCV and ubiquitinated by SidC/SdcA during *L. pneumophila* infection

As previously shown (Hoffmann et al., 2014), Rab10 is recruited to the LCV in a Dot/Icm-dependent manner (Fig. 5A, B). Since we find Rab10 is required for *L. pneumophila* pathogenesis, we sought to elucidate which *L. pneumophila* effectors are responsible for this recruitment. By using a panel of *L. pneumophila* strains with deletions in five gene clusters (2, 3, 4, 6, 7) encoding 31% of secreted effectors (O'Connor et al., 2011), we found that only strains with a deletion of gene cluster 7 (Δ7) were deficient in their ability to recruit GFP-Rab10 to the LCV in HeLa FcγRII cells (Fig. S5D, E). Gene cluster 7 contains nine secreted effectors (Fig. S5F). Due to their known role in recruiting ER proteins to the LCV (Horenkamp et al., 2014; Hsu et al., 2014; Ragaz et al., 2008), we focused on the paralogs SidC and SdcA as promising candidates for Rab10 recruitment to the LCV. Indeed, strains specifically lacking both *sidC* and *sdcA* (ΔsidC-sdcA) were unable to recruit GFP-Rab10, but this effect could be rescued in ΔsidC-sdcA *L. pneumophila* complemented with a plasmid expressing either effector (Figs. 5A, B).

As SidC/SdcA have been shown to be involved in the ubiquitination of other Rab proteins such as Rab1 (Horenkamp et al., 2014; Hsu et al., 2014), we tested whether *L. pneumophila* was hijacking Rab10 through a similar mechanism. We infected HEK293 FcγRII cells with either WT or ΔdotA *L. pneumophila* for 1 or 8 hours and analyzed cellular protein abundance and ubiquitination by mass spectrometry. Rab10 ubiquitination was significantly induced by WT *L. pneumophila* infection, with a ~36-fold increase at 1 hpi compared to

uninfected cells (Fig. 5C). This difference drops to ~7.5-fold by 8 hpi. Meanwhile, *dotA L. pneumophila* did not induce Rab10 ubiquitination at any timepoint. Interestingly, the increase in Rab10 ubiquitination by WT *L. pneumophila* had no effect on Rab10 protein abundance, suggesting the function of Rab10 ubiquitination by *L. pneumophila* is not linked to proteasomal degradation (Fig. 5D). We confirmed Rab10 ubiquitination by SidC/SdcA via immunoblot. Infection with WT *L. pneumophila* induced mono- and polyubiquitination of 3xFLAG-Rab10 whereas the *dotA* and *sidC-sdcA* strains did not (Fig. 5E). Meanwhile, complementation of the *sidC-sdcA* strain with a vector expressing SdcA driven by a strong *tac* promoter restored the ability of *L. pneumophila* to ubiquitinate Rab10 (Fig. 5E). Furthermore, an alternative strategy for complementing the *sidC-sdcA* deletion by transfecting HEK293 FcγRII cells with a plasmid expressing FLAG-SdcA was able to partially restore Rab10 ubiquitination while FLAG-SdcA $_C$, a truncated mutant lacking the C domain (residues 222–315) previously shown to be necessary for Rab1a ubiquitination (Horenkamp et al., 2014), was not (Fig. 5E).

The mass spectrometry additionally revealed that Rab10 was ubiquitinated at lysines K102, K136, and K154 (Fig. 5F). Of note, K154 is a part of the "SAK" motif in the G5 box that is conserved across guanine nucleotide binding proteins, necessary for guanine nucleotide binding (Pai et al., 1990), and mono-ubiquitination of this site regulates the activity of other Ras family GTPases (Baker et al., 2013; Sasaki et al., 2011). However, mutating K154 to an alanine had no effect on Rab10 recruitment to the LCV (Fig. S5G). Further studies will be necessary to completely elucidate the function of ubiquitination to control Rab10 activity, though our data show that *RABIF* and *RAB10* are required for *L. pneumophila* replication and LCV maturation, and that Rab10 is recruited to the LCV in a manner which requires SidC/SdcA.

Discussion:

Here we performed a host-targeted CRISPR-Cas9 genome-wide screen and secondary targeted screens to identify hundreds of genetic modifiers of *L. pneumophila* pathogenesis in human U937 cells. In addition to uncovering genes involved in phagocytosis and ER-to-Golgi trafficking known to be critical for *L. pneumophila* uptake and LCV maturation, respectively, we also revealed a large set of genes and pathways that have not previously been implicated in *L. pneumophila* pathogenesis. We demonstrated a role for two uncharacterized genes *C1orf43* and *KIAA1109* as regulators of phagocytosis. Additionally, we identified *RAB10* and its regulator *RABIF* as key modifiers of *L. pneumophila* replication and ER recruitment to the LCV. Further investigation revealed that Rab10 is recruited to the LCV and ubiquitinated by the *L. pneumophila* effectors SidC/SdcA.

Validating a panel of genes that were hits in both undifferentiated and differentiated U937 batch retest screens, we demonstrated that screen hits span various stages of *L. pneumophila* pathogenesis, including uptake by phagocytosis, LCV formation and maturation, and intracellular replication. Two of the top hits, *RABIF* and *RAB10*, regulate ER recruitment to the LCV and *L. pneumophila* replication. RABIF was recently discovered in a CRISPR screen for insulin-stimulated GLUT4 exocytosis in adipocytes (Gulbranson et al., 2017) as a chaperone that stabilizes Rab10. Here, we show that RABIF plays a similar role during *L.*

pneumophila infection, and that Rab10 activity is hijacked by *L. pneumophila* effectors. Rab10 is recruited to the LCV and also mono- and polyubiquitinated by the effectors SidC/ SdcA. Although Rab10 ubiquitination at K154 has not been seen before, mono- ubiquitination at the homologous residue K147 in KRAS has been shown to stabilize KRAS in the GTP-bound state by blocking GTPase-activating proteins (GAP)-mediated GTP hydrolysis (Baker et al., 2013; Sasaki et al., 2011). This in turn allows KRAS to more efficiently bind and activate key downstream effectors such as RAF kinases and phosphatidylinositol 3-kinase (PI3K) (Sasaki et al., 2011).

L. pneumophila is known to recruit key host factors that drive LCV remodeling and replication and tightly regulate their activity through post-translational modifications (e.g. Rab1) (Hardiman et al., 2012). Consistent with this general strategy, our data now suggest that Rab10 signaling at the LCV is a key driver of *L. pneumophila* pathogenesis. Rab10 has multiple known functions including exocytic trafficking via the exocyst complex (Sano et al., 2015), endocytic recycling (Babbey et al., 2006), and regulation of ER morphology (English and Voeltz, 2013). Future studies will be needed to dissect which function of Rab10 is being subverted by *L. pneumophila* and which Rab10 effectors are responsible for promoting intracellular replication. Because Rab10 regulates *L. pneumophila* replication in both differentiated and undifferentiated U937 cells while the exocyst complex only affects replication in undifferentiated U937 cells (Figs. 4A, S4C), we believe that Rab10 is not acting through the exocyst complex in this context.

Numerous other genes and processes revealed by the screens likely play diverse roles in *L. pneumophila* pathogenesis and warrant further investigation. For example, *C10orf76*, which we showed regulates *L. pneumophila* replication, was recently discovered as a phosphatidylinositol 4-kinase β (PI4KB) adaptor, deletion of which reduced phosphatidylinositol 4-phosphate [PI(4)P] levels in the cell and inhibited enterovirus replication (Blomen et al., 2015). During *L. pneumophila* infection, the LCV is remodeled into a PI(4)P-rich compartment (Weber et al., 2006), and key effectors such as SidC/SdcA have PI(4)P-binding domains that allow them to anchor to the LCV membrane and facilitate ER recruitment (Ragaz et al., 2008). It is not fully understood how PI(4)P is acquired on the LCV membrane, and *C10orf76* may be a novel regulator of this process.

Much of how the LCV avoids fusion with endolysosomes, as well as how it recruits and fuses with ER vesicles and membranes remains poorly understood. We expect that the numerous genes identified here involved in endosome, ER, and Golgi function and trafficking represent promising candidates for further exploration and should add to our understanding of *L. pneumophila* pathogenesis.

In summary, our genome-wide CRISPR screen revealed hundreds of host factors and diverse processes that both promote and restrict *L. pneumophila* pathogenesis in human cells. This comprehensive analysis provides a powerful resource for facilitating our understanding of *L. pneumophila* host-pathogen interactions and more broadly mammalian cell biology pathways such as phagocytosis and membrane trafficking. We have also established a successful screening paradigm that can be applied to many other pathogens that manipulate host machinery in different ways.

STAR Methods

LEAD CONTACT AND MATERIALS AVAILABILITY

Further information and requests for resources and reagents should be directed to and will be fulfilled by the Lead Contact, Michael Bassik (bassik@stanford.edu). Plasmids generated during this study have been deposited to Addgene.

EXPERIMENTAL MODEL AND SUBJECT DETAILS

Cell culture—U937 cells (ATCC) were cultured in RPMI-40 (Gibco) medium supplemented with 10% heat-inactivated FBS (Hyclone), penicillin (10,000 I.U./mL), streptomycin (10,000 g/mL). U937 cells were differentiated into macrophage-like cells by treating the cells with 50 nM Phorbol 12-myristate 13-acetate (PMA) for 3 days and then replating the cells in fresh media without PMA for 2 days. HeLa cells and human embryonic kidney (HEK293) cells stably expressing the FcγRII receptor were grown in DMEM (Gibco) supplemented with 10% FBS, penicillin, streptomycin, and L-glutamine (2 mM), as well as 150 μg/ml hygromycin B to maintain expression of the FcγRII receptor. Raw 264.7 cells (ATCC) were grown in DMEM supplemented with 10% heat-inactivated FBS, penicillin, and streptomycin. Cells were passaged by detaching the cells with a disposable cell scraper. All cell lines were maintained in logarithmic growth in a controlled humidifier at 37°C with 5% CO_2.

Bacterial strains and infections—All *L. pneumophila* strains unless otherwise noted are a gift from Craig Roy's lab at Yale University. All *L. pneumophila* strains were grown on Charcoal Yeast Extract (CYE) agar plates or AYE broth as previously described. Experiments were performed with *Legionella pneumophila* serogroup 1, strain Lp01 unless otherwise noted. The *dotA*, *sidC-sdcA*, and IPTG-inducible mCherry-expressing strains were derived from the parental Lp01 strain as described previously (Berger et al., 1994). The *sidC-sdcA* and mCherry *L. pneumophila* strains were grown with chloramphenicol. 2,3,4,6,7, 2,3,6,7, 2,3,6, and 7 *L. pneumophila* strains (O'Connor et al., 2011) are derived from the *Legionella pneumophila* serogroup 1 strain Lp02 (Berger and Isberg, 1993) and are thymidine auxotrophs. Chloramphenicol (10 ug/mL), IPTG (0.1 mM), and thymidine (100 ug/mL) were added to CYE agar plates as needed. Aside from the intracellular replication assays, *L. pneumophila* were harvested from 2-day heavy patches and used to infect cells. When infecting U937 and Raw 264.7 cells, bacteria were added directly to the cells. When infecting HeLa FcγRII and HEK293 FcγRII cells, bacteria were first opsonized with anti-*Legionella* antibody at 1:2000 dilution for 20 min on a rotator before being added to cells. Cells were then centrifuged for 1000 × g for 5 min and incubated at 37°C for the desired amount of time.

METHOD DETAILS

Antibodies—Rabbit polyclonal anti-*Legionella* antibody (PA1–7227, Thermo Fisher Scientific, 1:2000 dilution) and mouse polyclonal anti-*Legionella* antibody [gift from Kohei Arasaki (Arasaki and Roy, 2010), 1:2000 dilution] were used to opsonize *L. pneumophila* for infections and immunofluorescence assays. Rabbit polyclonal anti-Nogo A+B antibody (ab47085, Abcam, 1:200 dilution), mouse monoclonal anti-Cytochrome C antibody

(556432, BD, 1:800 dilution), mouse monoclonal anti-GM130 antibody (610822, BD, 1:500 dilution), and mouse monoclonal anti-LAMP1 antibody (#15665, Cell Signaling Technology, 1:100 dilution) were used for immunofluorescence assays. Rabbit monoclonal anti-FLAG antibody (#14793, Cell Signaling Technology, 1:800 dilution), mouse monoclonal anti-FLAG antibody (F1804, Sigma-Aldrich, 1:800 dilution), mouse monoclonal anti-RABIF antibody (sc-390759, Santa Cruz Biotechnology, 1:1000 dilution), rabbit monoclonal anti-Rab10 antibody (#8127, Cell Signaling Technology, 1:600 dilution), rabbit polyclonal anti-Rab1A antibody (sc-311, Santa Cruz Biotechnology, 1:200 dilution), and mouse monoclonal anti-GAPDH antibody (AM4300, Thermo Fisher Scientific, 1:4000 dilution) were used for western blotting.

Generation of individual sgRNA-expressing cells/ stable cell lines—Lentivirus production and infection were performed as previously described (Morgens et al., 2016). Briefly HEK293T cells were transfected with third-generation packaging plasmids and the sgRNA-expressing vector. Lentivirus was harvested after 48 h and 72 h and filtered through a 0.45μm Polyvinylidene Fluoride (PVDF) filter (Millipore). U937 cells expressing lentiCas9-Blast(Sanjana et al., 2014) were infected by centrifugation at $1000 \times g$ for 2 h. Raw 264.7 expressing UCOE-EF-1α-Cas9-BFP (Haney et al., 2018) and HeLa FcγRII cells expressing lentiCas9-Blast were infected by incubating the cells in lentivirus-containing media for 24 h. 3 days after infection, cells were selected with puromycin (1 μg/mL for 3 d for U937 and HeLa FcγRII cells, 10 μg/mL for 5 d for Raw 264.7 cells). When necessary, clonal knockout lines were generated by single-cell sorting puromycin-selected cells into 96-well plates and expanding them for 2–3 weeks. Gene editing efficiency was determined by Sanger sequencing and analyzing the resulting chromatograms using TIDE software (Brinkman et al., 2014).

Genome-wide CRISPR-Cas9 Screen—The genome-wide CRISPR-Cas9 library containing 10 sgRNAs per gene was synthesized and infected into Cas9-expressing U937 cells as previously described (Morgens et al., 2017). Briefly, U937 cells stably expressing lentiCas9-Blast (Sanjana et al., 2014) were lentivirally infected with the genome-wide sgRNA library. After 3 days, we applied puromycin selection (1 μg/mL) for 3 days until >90% of the population contained the library (determined by mCherry expression). At the start of the screen, cells were split into two conditions – one population was treated with 5 rounds of WT *L. pneumophila* infection over 18 days and the other untreated control population was maintained in log-phase growth throughout the duration of the screen. The screen was performed at 1000X coverage (cells were kept at above 250×10^6 cells in a 500 mL culture) in large spinner flasks. For each round of *L. pneumophila* infection, 25×10^9 *L. pneumophila* (MOI = 100) were harvest from 2-day heavy patches and resuspended in 180 mL media. 250×10^6 U937 cells were pelleted and then resuspended with the *L. pneumophila*-containing media and transferred to 6-well plates with 5 mL of cells per well. Plates were centrifuged at 1000 rpm for 15 minutes to infect cells with *L. pneumophila*. Plates were incubated for 1 hour at 37°C before transferring the cells back into spinner flasks. 24 hours after infection, the antibiotic rifampicin (10 μg/mL) was added to kill remaining bacteria and cells were allowed to recover to ~90% viability before the subsequent round of *L. pneumophila* infection. At the end of the screen, genomic DNA was

extracted from each population using the Qiagen Blood Maxi Kit and the guide frequencies were quantified by deep sequencing using an Illumina NextSeq 500.

Batch retest CRISPR-Cas9 Screens—The batch retest mini-library contains ~12,400 sgRNAs and consists of 10 sgRNAs per gene targeting 1139 genes and 1000 negative control sgRNAs, synthesized and cloned as previously described (Morgens et al., 2017). The genes were chosen to include the 200 genes with the highest confidence scores from the genome-wide CRISPR screen, genes encoding proteins found in the LCV (Hoffman, 2014), and additional genes involved in vesicle trafficking. The screen in undifferentiated U937 cells was conducted in the same way as the genome-wide screen except at 4000X coverage (50×10^6 cells in a 100 mL culture) in T-150 flasks in duplicate. For the PMA-differentiated U937 screen, also performed in duplicate, 100×10^6 cells were differentiated in 100 mL media in 15 cm tissue culture dishes for an 8000X initial coverage. On the day of infection, media was aspirated from each dish and 6×10^9 WT *L. pneumophila* (MOI = 60) harvested from a 2-day heavy patch were resuspended in 100 mL media and added to each dish and allowed to infect for 24 hours, resulting in ~80% cell death. Uninfected control samples received fresh media without *L. pneumophila*. Libraries were prepared and sequenced as in the genome-wide screen.

Analysis of CRISPR-Cas9 screens—The genome-wide screen was analyzed using casTLE version 1.0 as previously described (Morgens et al., 2016). Briefly, the distribution of guides was compared between the uninfected and *L. pneumophila*-infected samples and guide enrichments were calculated as log ratios between the infected and uninfected samples. A maximum likelihood estimator was used to estimate the effect size for each gene and the log-likelihood ratio (confidence score, or casTLE score) by comparing the distribution of the 10 gene-targeting guides to the distribution of negative control guides. An effect size of 1 roughly corresponds to one log2 fold change of the gene compared to the negative controls. *P* values were determined by permuting the gene-targeting guides in the screen and comparing to the distribution of negative controls using casTLE, and FDR thresholds for defining hits were calculated using the Benjamini-Hochberg procedure. For the genome-wide screen, we used a threshold of 10% FDR to define hits. GO terms were generated using GOrilla on the gene list ranked by confidence score (Eden et al., 2009).

For the batch retest screens, effect scores and confidence scores were calculated using casTLE version 1.0 as in the genome-wide screen, and the results of the two replicates for each screen were combined. Because the batch retest library is highly enriched for genes involved in *L. pneumophila* pathogenesis, calculating *P* values as in the genome- wide by permuting targeting guides is less appropriate for the batch retest library. Instead, genes were called as hits when their combination effect score at 95% credible interval did not include zero (Haney et al., 2018; Kramer et al., 2018; Liu et al., 2018). Intuitively, it is similar to using a *P* value threshold of p<0.05. Here, we use the casTLE framework to evaluate a posterior distribution of the effect size, which we can use to estimate the 95% credible interval (the shortest interval which contains 95% of the weight of the posterior distribution). This gives us an effective measurement of the noise in our estimated effect size, allowing us to ask whether a gene has an effect in the batch screens.

In general, sgRNAs with the strongest effects in the screens were chosen for follow-up experiments. All sgRNAs used in this study are listed in Table S5.

Competitive killing assay—U937 cells stably expressing Cas9 were infected with a plasmid expressing sgRNAs targeting each gene of interest and GFP or a plasmid expressing a negative control sgRNA and mCherry. After selection with puromycin (1 μg/mL), mCherry-positive and GFP-positive cells were co-cultured in equal numbers and infected with *L. pneumophila* at MOI = 100 in triplicate and the number of cells with each fluorophore was measured using an Incucyte Zoom (Essen Bioscience). After 24 hours, rifampicin (10 μg/mL) was added to kill all bacteria. The change in the percentage of GFP-positive cells between the 48 h and 0 h timepoints was compared between *L. pneumophila*-infected cells and uninfected control cells.

For C1orf43 rescue experiments, GFP-positive C1orf43 clonal knockout cells or negative control cells were lentivirally infected with plasmids expressing C1orf43–3xFLAG, C1orf43$_{1-41}$-3xFLAG, or a negative control vector followed by G418 selection (700 μg/ml) for 7 d. Cells were then mixed with cells expressing a negative control sgRNA and mCherry and the competitive killing assay was performed as before.

Phagocytosis assay— dotA *L. pneumophila* were harvested from a 2-day heavy patch and conjugated to pHrodo Red succinimidyl ester dye (Thermo Fisher Scientific) following manufacturer's protocols. Briefly, 2×10^9 bacteria were resuspended in 750 μl 0.1 M NaHCO$_3$, pH 8.3, mixed with 38 μl of 10 mM pHrodo Red dye, and incubated in the dark for 45 minutes at room temperature. Bacteria were then washed 4 times with 750 μl Hank's Balanced Salt Solution (HBSS) and resuspended in 1 ml sterile water. Bacteria were transferred into 1.5 ml tubes with 100×10^6 CFUs per aliquot and lyophilized using a Freezone 4.5 Liter Benchtop Freeze Dry System (Labconco). After lyophilization, aliquots of pHrodo Red-labeled dotA *L. pneumophila* were stored in −20°C until use. For the phagocytos is assay, pHrodo Red-labeled bacteria were resuspended in DMEM media with 10% FBS and added to 50,000 GFP+ differentiated U937 knockout cells in a 96-well plate at MOI = 10 in quadruplicate. Plates were centrifuged at 1000×g for 5 minutes and then imaged in an Incucyte Zoom (Essen Bioscience) every hour for 6 hours using a 10X objective with 4 images taken per well. Phagocytic index was calculated as the total mCherry intensity normalized to the number of GFP+ cells. Phagocytosis assays in Raw 264.7 cells were performed similarly except 50,000 colorless Raw 264.7 knockout cells were plated per well one day before infection and phagocytic index was calculated as total mCherry intensity.

For other phagocytic substrates, pHrodo Red *E. coli* or *S. aureus* BioParticles conjugates (Thermo Fisher Scientific) were resuspended in media, diluted to 0.025 mg/mL, and 100 uL of the diluted substrate was added per well. Zymosan (Sigma, Z4250), a yeast cell wall particle, and amino magnetic 1.12 μm-diameter polystyrene beads (Spherotech AM-10–10) were conjugated to pHrodo Red succinimidyl ester (Thermo Fisher) Scientific as previously described (Haney et al., 2018). Labeled zymosan was used at a final concentration of 0.0188 mg/mL and labeled beads were used at a final concentration of 0.00625% w/v.

***L. pneumophila* intracellular replication assay**—*L. pneumophila* expressing mCherry were harvested from a two-day heavy patch, diluted to 0.1–0.3 OD, and grown to post-exponential phase overnight in AYE broth with chloramphenicol (10 ug/mL) and IPTG (1 mM) to induce mCherry expression. Bacteria were then added to $0.2{\times}10^6$ undifferentiated U937 knockout cells at MOI = 4 or $0.5{\times}10^6$ differentiated U937 knockout cells at MOI = 1 in media containing 1 mM IPTG in 24-well plates in at least triplicate. Plates were imaged in an Incucyte S3 (Essen Bioscience) at regular intervals for 36 h (for differentiated U937 cells) or 72 h (for undifferentiated U937 cells) using a 4X objective with 4 images taken per well. The total red intensity per well was used to measure *L. pneumophila* burden.

Immunofluorescence microscopy—HeLa FcγRII cells were plated on 12 mm glass coverslips in 24-well plates. After 24 hours, cells were fixed, treated with drugs, or infected with *L. pneumophila* as needed. For RTN4 recruitment assays, HeLa FcγRII cells were infected with *L. pneumophila* at MOI = 1 in triplicate. 1 h after infection, cells were washed twice with PBS to remove extracellular bacteria and incubated for 3 h more. For LAMP1 co-localization assay, HeLa FcγRII cells were infected with *L. pneumophila* at MOI = 3 and infected for 1, 4, or 8 h. For 4 and 8 h timepoints, cells were washed with PBS after 1 h to remove extracellular bacteria. For GFP-Rab10 recruitment assays, HeLa FcγRII cells stably expressing GFP-Rab10 were infected with the indicated *L. pneumophila* strains at MOI = 3 for 1 h in triplicate. Cells were washed with cold dPBS, fixed with 4% paraformaldehyde in PBS for 10 min at room temperature, permeabilized in 0.1% Triton X-100 in PBS, and blocked in 3% bovine serum albumin (BSA) in PBS, and then incubated with the appropriate primary and secondaries antibodies diluted in 3% BSA. Nuclei were stained with Hoechst 33342 dye for 10 min before mounting on microscope slides. Coverslips were imaged using an inverted Nikon Eclipse Ti-E spinning disk confocal microscope and an Andor Ixon3 EMCCD camera or a Leica TCS SP5 confocal microscope at 60X or 100X magnification. For co-localization experiments, individual intracellular *L. pneumophila* were quantified.

Live cell microscopy for C1orf43-GFP localization during *L. pneumophila* infection—HeLa FcγRII cells stably expressing C1orf43-GFP were plated on 35 mm poly-lysine-coated imaging dishes (Cellvis). Cells were infected at MOI = 2 with WT *L. pneumophila* that were previously stained with HaloTag-Janelia Fluor 646 conjugates (Grimm et al., 2017). For staining, briefly, *L. pneumophila* maintaining a HaloTag-expressing plasmid were harvested from a 2-day heavy patch and incubated at liquid culture overnight with 0.1 mM IPTG. Liquid culture at OD = 3.0 was then pelleted and resuspended in 5 μM Janelia Fluor 646 HaloTag ligand (JF646) in order to facilitate HaloTag-JF646 conjugation. After a 15 min incubation with ligand in the dark, *L. pneumophila* were washed 1x with water. Stained bacteria were resuspended in 2 mL of DMEM lacking phenol red (Gibco) and used for infection of cells. Imaging of cells took place in a controlled chamber maintaining 37°C with 5% CO_2. A random selection of cells were imaged at 60X magnification at 1 minute intervals for 50 minutes using a Nikon Eclipse Ti2 microscope with a Nikon DS-Qi2 camera.

Affinity purification and mass spectrometry for RABIF interactors—600×10^6 U937 cells stably expressing GFP-RABIF or a GFP control were collected in triplicate, washed with PBS, and lysed in NP-40 lysis buffer (50 mM HEPES-KOH pH 6.8, 500 μM EGTA, pH 6.8, 150 mM KCl, 2 mM $MgCl_2$, 1 mM $CaCl_2$, 15% glycerol, 0.3% NP-40, and protease inhibitors, EDTA-free, Roche) by nutating for 45 min at 4°C. Lysates were clarified at 25,000 RPM for 20 min at 4°C in a Sw41 Ti rotor. Lysates were immunoprecipitated using anti-GFP beads (Chromotek) for 1 h at 4°C. Beads were washed 3 times with wash buffer (lysis buffer with 0.05% NP-40) and 3 times with buffer without NP-40. Purified proteins were predigested in 38 μl 50 mM Tris-HCl, pH 7.5, 2M urea, 200 ng Sequencing Grade Modified Trypsin (Promega), 1 mM DTT for 30 min at room temperature. Supernatants were collected, and proteins were further eluted by adding 70 μl 50 mM Tris-HCl, pH 7.5, 2M urea, 5 mM chloroacetamide two times and combining with the original supernatant. Proteins were digested overnight and digestion was stopped by adding 1.5 μl 1% (v/v) trifluoroacetic acid. Samples were dried in a SpeedVac and the pellet was resuspended in 0.1% acetic acid and desalted on C18 StageTips. Next, samples were dried in a SpeedVac and resuspended in 100 mM ammonium formate.

The cleaned protein digest was introduced to a Waters Liquid Chromatography column coupled to an Orbitrap Fusion mass spectrometer (Thermo Fisher Scientific). Peptides were separated using a 25 cm long and 100 μm inner diameter capillary column packed with Sepax 1.8 μm C18 resin. Peptides were eluted off in a 60 minute gradient at a flow rate of 600 nl/min from 5% to 35% acetonitrile in 0.1% formic acid. Mass spectrometry data was acquired by one full MS scan at 120k resolution followed with MS2 using HCD at 30k resolution. The instrument was set to run in top speed mode with 3 s cycle. Raw data was processed using Thermo Proteome Discoverer software version 2.2. MS data were searched against a human proteome database with 1% FDR at the peptide level. Protein quantification was based on the precursor ion peak intensity using the label-free quantitation workflow. Peptide spectral match (PSM) counts from three replicates of GFP-RABIF samples were compared against three replicates of GFP control samples to generate SAINT confidence scores and fold changes (Choi et al., 2011).

Mass spectrometry for Rab10 ubiquitination and abundance—72×10^6 HEK293 FcγRII cells were infected with WT or *dotA L. pneumophila* at MOI = 100 for 1 h or 8 h in triplicate. Cells were lysed by sonication in 8M urea, 0.1 M Ammonium Bicarbonate (ABC) pH 8.0, 150 mM NaCl, and protease and phosphatase inhibitors (Mini Complete tablet of each from Roche for 10 ml buffer). Reduction of disulfide bonds was achieved by addition of 4 mM TECP for 30 min at RT, follow by alkylation with 10mM iodoacetamide and incubation at RT for 30 min in the dark. The reaction was then quenched by the addition of 10mM DTT and incubation at RT in the dark for 30min. Next, 100 mM ABC pH 8 was added to dilute the solution to a final concentration of 2 M urea. 100 μg of trypsin was then added to ~7 mg of protein and incubated at 37°C overnight. The resulting peptides were desalted on tC18 Sep-Paks, lyophilized, and a 20 μg aliquot removed for analysis of protein abundance. The remaining protein was enriched for diglycine remnant peptides, indicative of ubiquitin attachment, with an anti-diglycine remnant antibody (Cell Signaling Technologies) as previously described (Udeshi et al., 2013), and the resulting diglycine peptides were

desalted in micro C18 columns. Both aliquots (protein abundance and diglycine enriched) were resuspended in 4% formic acid, 4% acetonitrile solution, and peptides were directly injected into an Orbitrap Fusion Lumos Tribrid Mass Spectrometer (Thermo). Diglycine peptides were separated by a 70 minute reversed-phase gradient over a nanoflow C18 column (Dr. Maisch) and MS1 and MS2 spectra collected in the orbitrap, while aliquots for protein abundance analysis were separated by a 120 minute reversed-phase gradient with MS1 spectra collected in the orbitrap, and MS2 spectra in the ion trap. All raw MS data was searched using MaxQuant (Cox and Mann, 2008), and label-free quantification and statistical analysis was performed using MSstats (Choi et al., 2014).

Immunoblot analysis—Whole-cell protein extracts were prepared using lysis buffer containing 50 mM Tris-HCl pH 7.5, 150 mM NaCl, 1 mM EDTA, and 1% Triton X-100 supplemented with Protease Inhibitor Cocktail (Sigma-Aldrich). Lysates were centrifuged at 15,000 × g for 10 min at 4°C to remove cellular debris. Samples were separated by SDS-PAGE, transferred to nitrocellulose membranes, and immunoblotted according to standard protocols using the Li-Cor Odyssey Infrared Imaging System or Supersignal West Duro Extended Duration ECL substrate with a Bio-Rad Chemidoc system.

QUANTIFICATION AND STATISTICAL ANALYSIS

Statistical analyses were performed using GraphPad Prism 7. Automated quantification of phagocytosis and *L. pneumophila* intracellular replication images were performed using Incucyte Zoom and S3 software (Essen). Image analysis was performed using ImageJ. Statistical details of experiments can be found in the figure legends. Network diagrams were generated using Cytoscape v3.7. Rab10 protein structure was generated using PyMOL. Randomization, blinding, and sample-size estimation were not applicable in this study.

DATA AND CODE AVAILABILITY

Sequencing data are available at Sequence Read Archive (SRA) accession number SRP202048 under BioProject accession number PRJNA549978.

Supplementary Material

Refer to Web version on PubMed Central for supplementary material.

Acknowledgments

References

Adamson B, Norman TM, Jost M, Cho MY, Nunez JK, Chen Y, Villalta JE, Gilbert LA, Horlbeck MA, Hein MY, et al. (2016). A Multiplexed Single-Cell CRISPR Screening Platform Enables Systematic Dissection of the Unfolded Protein Response. Cell 167, 1867–1882 e1821. [PubMed: 27984733]

Arasaki K, Kimura H, Tagaya M, and Roy CR (2018). Legionella remodels the plasma membrane-derived vacuole by utilizing exocyst components as tethers. J Cell Biol 217, 3863–3872. [PubMed: 30275106]

Arasaki K, and Roy CR (2010). Legionella pneumophila promotes functional interactions between plasma membrane syntaxins and Sec22b. Traffic 11, 587–600. [PubMed: 20163564]

Babbey CM, Ahktar N, Wang E, Chen CC, Grant BD, and Dunn KW (2006). Rab10 regulates membrane transport through early endosomes of polarized Madin-Darby canine kidney cells. Mol Biol Cell 17, 3156–3175. [PubMed: 16641372]

Baker R, Lewis SM, Sasaki AT, Wilkerson EM, Locasale JW, Cantley LC, Kuhlman B, Dohlman HG, and Campbell SL (2013). Site-specific monoubiquitination activates Ras by impeding GTPase-activating protein function. Nat Struct Mol Biol 20, 46–52. [PubMed: 23178454]

Banga S, Gao P, Shen X, Fiscus V, Zong WX, Chen L, and Luo ZQ (2007). Legionella pneumophila inhibits macrophage apoptosis by targeting pro-death members of the Bcl2 protein family. Proc Natl Acad Sci U S A 104, 5121–5126. [PubMed: 17360363]

Bassik MC, Kampmann M, Lebbink RJ, Wang S, Hein MY, Poser I, Weibezahn J, Horlbeck MA, Chen S, Mann M, et al. (2013). A systematic mammalian genetic interaction map reveals pathways underlying ricin susceptibility. Cell 152, 909–922. [PubMed: 23394947]

Berger KH, and Isberg RR (1993). Two distinct defects in intracellular growth complemented by a single genetic locus in Legionella pneumophila. Mol Microbiol 7, 7–19. [PubMed: 8382332]

Berger KH, Merriam JJ, and Isberg RR (1994). Altered intracellular targeting properties associated with mutations in the Legionella pneumophila dotA gene. Mol Microbiol 14, 809–822. [PubMed: 7891566]

Bhogaraju S, Kalayil S, Liu Y, Bonn F, Colby T, Matic I, and Dikic I (2016). Phosphoribosylation of Ubiquitin Promotes Serine Ubiquitination and Impairs Conventional Ubiquitination. Cell 167, 1636–1649 e1613. [PubMed: 27912065]

Blomen VA, Majek P, Jae LT, Bigenzahn JW, Nieuwenhuis J, Staring J, Sacco R, van Diemen FR, Olk N, Stukalov A, et al. (2015). Gene essentiality and synthetic lethality in haploid human cells. Science 350, 1092–1096. [PubMed: 26472760]

Botelho RJ, Teruel M, Dierckman R, Anderson R, Wells A, York JD, Meyer T, and Grinstein S (2000). Localized biphasic changes in phosphatidylinositol-4,5-bisphosphate at sites of phagocytosis. J Cell Biol 151, 1353–1368. [PubMed: 11134066]

Brinkman EK, Chen T, Amendola M, and van Steensel B (2014). Easy quantitative assessment of genome editing by sequence trace decomposition. Nucleic Acids Res 42, e168. [PubMed: 25300484]

Choi H, Larsen B, Lin ZY, Breitkreutz A, Mellacheruvu D, Fermin D, Qin ZS, Tyers M, Gingras AC, and Nesvizhskii AI (2011). SAINT: probabilistic scoring of affinity purification-mass spectrometry data. Nat Methods 8, 70–73. [PubMed: 21131968]

Choi M, Chang CY, Clough T, Broudy D, Killeen T, MacLean B, and Vitek O (2014). MSstats: an R package for statistical analysis of quantitative mass spectrometry-based proteomic experiments. Bioinformatics 30, 2524–2526. [PubMed: 24794931]

Choy A, Dancourt J, Mugo B, O'Connor TJ, Isberg RR, Melia TJ, and Roy CR (2012). The Legionella effector RavZ inhibits host autophagy through irreversible Atg8 deconjugation. Science 338, 1072–1076. [PubMed: 23112293]

Cox D, Lee DJ, Dale BM, Calafat J, and Greenberg S (2000). A Rab11-containing rapidly recycling compartment in macrophages that promotes phagocytosis. Proc Natl Acad Sci U S A 97, 680–685. [PubMed: 10639139]

Cox J, and Mann M (2008). MaxQuant enables high peptide identification rates, individualized p.p.b.-range mass accuracies and proteome-wide protein quantification. Nat Biotechnol 26, 1367–1372. [PubMed: 19029910]

de Jesus-Diaz DA, Murphy C, Sol A, Dorer M, and Isberg RR (2017). Host Cell S Phase Restricts Legionella pneumophila Intracellular Replication by Destabilizing the Membrane-Bound Replication Compartment. MBio 8.

Derre I, and Isberg RR (2004). Legionella pneumophila replication vacuole formation involves rapid recruitment of proteins of the early secretory system. Infect Immun 72, 3048–3053. [PubMed: 15102819]

Dorer MS, Kirton D, Bader JS, and Isberg RR (2006). RNA interference analysis of Legionella in Drosophila cells: exploitation of early secretory apparatus dynamics. PLoS Pathog 2, e34. [PubMed: 16652170]

Eden E, Navon R, Steinfeld I, Lipson D, and Yakhini Z (2009). GOrilla: a tool for discovery and visualization of enriched GO terms in ranked gene lists. BMC Bioinformatics 10, 48. [PubMed: 19192299]

English AR, and Voeltz GK (2013). Rab10 GTPase regulates ER dynamics and morphology. Nat Cell Biol 15, 169–178. [PubMed: 23263280]

Grimm JB, Muthusamy AK, Liang Y, Brown TA, Lemon WC, Patel R, Lu R, Macklin JJ, Keller PJ, Ji N, et al. (2017). A general method to fine-tune fluorophores for live-cell and in vivo imaging. Nat Methods 14, 987–994. [PubMed: 28869757]

Gulbranson DR, Davis EM, Demmitt BA, Ouyang Y, Ye Y, Yu H, and Shen J (2017). RABIF/MSS4 is a Rab-stabilizing holdase chaperone required for GLUT4 exocytosis. Proc Natl Acad Sci U S A 114, E8224–E8233. [PubMed: 28894007]

Han K, Jeng EE, Hess GT, Morgens DW, Li A, and Bassik MC (2017). Synergistic drug combinations for cancer identified in a CRISPR screen for pairwise genetic interactions. Nat Biotechnol 35, 463–474. [PubMed: 28319085]

Haney MS, Bohlen CJ, Morgens DW, Ousey JA, Barkal AA, Tsui CK, Ego BK, Levin R, Kamber RA, Collins H, et al. (2018). Identification of phagocytosis regulators using magnetic genome-wide CRISPR screens. Nat Genet.

Hardiman CA, McDonough JA, Newton HJ, and Roy CR (2012). The role of Rab GTPases in the transport of vacuoles containing Legionella pneumophila and Coxiella burnetii. Biochem Soc Trans 40, 1353–1359. [PubMed: 23176480]

Hoffmann C, Finsel I, Otto A, Pfaffinger G, Rothmeier E, Hecker M, Becher D, and Hilbi H (2014). Functional analysis of novel Rab GTPases identified in the proteome of purified Legionella-containing vacuoles from macrophages. Cell Microbiol 16, 1034–1052. [PubMed: 24373249]

Horenkamp FA, Mukherjee S, Alix E, Schauder CM, Hubber AM, Roy CR, and Reinisch KM (2014). Legionella pneumophila subversion of host vesicular transport by SidC effector proteins. Traffic 15, 488–499. [PubMed: 24483784]

Horwitz MA (1983a). Formation of a novel phagosome by the Legionnaires' disease bacterium (Legionella pneumophila) in human monocytes. J Exp Med 158, 1319–1331. [PubMed: 6619736]

Horwitz MA (1983b). The Legionnaires' disease bacterium (Legionella pneumophila) inhibits phagosome-lysosome fusion in human monocytes. J Exp Med 158, 2108–2126. [PubMed: 6644240]

Horwitz MA, and Silverstein SC (1980). Legionnaires' disease bacterium (Legionella pneumophila) multiples intracellularly in human monocytes. J Clin Invest 66, 441–450. [PubMed: 7190579]

Hsu F, Luo X, Qiu J, Teng YB, Jin J, Smolka MB, Luo ZQ, and Mao Y (2014). The Legionella effector SidC defines a unique family of ubiquitin ligases important for bacterial phagosomal remodeling. Proc Natl Acad Sci U S A 111, 10538–10543. [PubMed: 25006264]

Hubber A, and Roy CR (2010). Modulation of host cell function by Legionella pneumophila type IV effectors. Annu Rev Cell Dev Biol 26, 261–283. [PubMed: 20929312]

Huttlin EL, Bruckner RJ, Paulo JA, Cannon JR, Ting L, Baltier K, Colby G, Gebreab F, Gygi MP, Parzen H, et al. (2017). Architecture of the human interactome defines protein communities and disease networks. Nature 545, 505–509. [PubMed: 28514442]

Ingmundson A, Delprato A, Lambright DG, and Roy CR (2007). Legionella pneumophila proteins that regulate Rab1 membrane cycling. Nature 450, 365–369. [PubMed: 17952054]

Kagan JC, and Roy CR (2002). Legionella phagosomes intercept vesicular traffic from endoplasmic reticulum exit sites. Nat Cell Biol 4, 945–954. [PubMed: 12447391]

Kagan JC, Stein MP, Pypaert M, and Roy CR (2004). Legionella subvert the functions of Rab1 and Sec22b to create a replicative organelle. J Exp Med 199, 1201–1211. [PubMed: 15117975]

Kane MS, Diamonstein CJ, Hauser N, Deeken JF, Niederhuber JE, and Vilboux T (2019). Endosomal trafficking defects in patient cells with KIAA1109 biallelic variants. Genes Dis 6, 56–67. [PubMed: 30906834]

Khuong TM, Habets RL, Slabbaert JR, and Verstreken P (2010). WASP is activated by phosphatidylinositol-4,5-bisphosphate to restrict synapse growth in a pathway parallel to bone morphogenetic protein signaling. Proc Natl Acad Sci U S A 107, 17379–17384. [PubMed: 20844206]

Koeffler HP (1983). Induction of differentiation of human acute myelogenous leukemia cells: therapeutic implications. Blood 62, 709–721. [PubMed: 6192859]

Koike-Yusa H, Li Y, Tan EP, Velasco-Herrera Mdel C, and Yusa K (2014). Genome-wide recessive genetic screening in mammalian cells with a lentiviral CRISPR-guide RNA library. Nat Biotechnol 32, 267–273. [PubMed: 24535568]

Kramer NJ, Haney MS, Morgens DW, Jovicic A, Couthouis J, Li A, Ousey J, Ma R, Bieri G, Tsui CK, et al. (2018). CRISPR-Cas9 screens in human cells and primary neurons identify modifiers of C9ORF72 dipeptide-repeat-protein toxicity. Nat Genet 50, 603–612. [PubMed: 29507424]

Liu N, Lee CH, Swigut T, Grow E, Gu B, Bassik MC, and Wysocka J (2018). Selective silencing of euchromatic L1s revealed by genome-wide screens for L1 regulators. Nature 553, 228–232. [PubMed: 29211708]

Luo ZQ, and Isberg RR (2004). Multiple substrates of the Legionella pneumophila Dot/Icm system identified by interbacterial protein transfer. Proc Natl Acad Sci U S A 101, 841–846. [PubMed: 14715899]

Mao Y, and Finnemann SC (2015). Regulation of phagocytosis by Rho GTPases. Small GTPases 6, 89–99. [PubMed: 25941749]

May RC, Caron E, Hall A, and Machesky LM (2000). Involvement of the Arp2/3 complex in phagocytosis mediated by FcgammaR or CR3. Nat Cell Biol 2, 246–248. [PubMed: 10783245]

Morgens DW, Deans RM, Li A, and Bassik MC (2016). Systematic comparison of CRISPR/Cas9 and RNAi screens for essential genes. Nat Biotechnol 34, 634–636. [PubMed: 27159373]

Morgens DW, Wainberg M, Boyle EA, Ursu O, Araya CL, Tsui CK, Haney MS, Hess GT, Han K, Jeng EE, et al. (2017). Genome-scale measurement of off-target activity using Cas9 toxicity in high-throughput screens. Nat Commun 8, 15178. [PubMed: 28474669]

Mukherjee S, Liu X, Arasaki K, McDonough J, Galan JE, and Roy CR (2011). Modulation of Rab GTPase function by a protein phosphocholine transferase. Nature 477, 103–106. [PubMed: 21822290]

Ninio S, and Roy CR (2007). Effector proteins translocated by Legionella pneumophila: strength in numbers. Trends Microbiol 15, 372–380. [PubMed: 17632005]

O'Connor TJ, Adepoju Y, Boyd D, and Isberg RR (2011). Minimization of the Legionella pneumophila genome reveals chromosomal regions involved in host range expansion. Proc Natl Acad Sci U S A 108, 14733–14740. [PubMed: 21873199]

Pai EF, Krengel U, Petsko GA, Goody RS, Kabsch W, and Wittinghofer A (1990). Refined crystal structure of the triphosphate conformation of H-ras p21 at 1.35 A resolution: implications for the mechanism of GTP hydrolysis. EMBO J 9, 2351–2359. [PubMed: 2196171]

Parnas O, Jovanovic M, Eisenhaure TM, Herbst RH, Dixit A, Ye CJ, Przybylski D, Platt RJ, Tirosh I, Sanjana NE, et al. (2015). A Genome-wide CRISPR Screen in Primary Immune Cells to Dissect Regulatory Networks. Cell 162, 675–686. [PubMed: 26189680]

Philips JA, Rubin EJ, and Perrimon N (2005). Drosophila RNAi screen reveals CD36 family member required for mycobacterial infection. Science 309, 1251–1253. [PubMed: 16020694]

Qiu J, Sheedlo MJ, Yu K, Tan Y, Nakayasu ES, Das C, Liu X, and Luo ZQ (2016). Ubiquitination independent of E1 and E2 enzymes by bacterial effectors. Nature 533, 120–124. [PubMed: 27049943]

Ragaz C, Pietsch H, Urwyler S, Tiaden A, Weber SS, and Hilbi H (2008). The Legionella pneumophila phosphatidylinositol-4 phosphate-binding type IV substrate SidC recruits endoplasmic reticulum vesicles to a replication-permissive vacuole. Cell Microbiol 10, 2416–2433. [PubMed: 18673369]

Rougerie P, Miskolci V, and Cox D (2013). Generation of membrane structures during phagocytosis and chemotaxis of macrophages: role and regulation of the actin cytoskeleton. Immunol Rev 256, 222–239. [PubMed: 24117824]

Rowbotham TJ (1980). Preliminary report on the pathogenicity of Legionella pneumophila for freshwater and soil amoebae. J Clin Pathol 33, 1179–1183. [PubMed: 7451664]

Sanjana NE, Shalem O, and Zhang F (2014). Improved vectors and genome-wide libraries for CRISPR screening. Nat Methods 11, 783–784. [PubMed: 25075903]

Sano H, Peck GR, Blachon S, and Lienhard GE (2015). A potential link between insulin signaling and GLUT4 translocation: Association of Rab10-GTP with the exocyst subunit Exoc6/6b. Biochem Biophys Res Commun 465, 601–605. [PubMed: 26299925]

Sasaki AT, Carracedo A, Locasale JW, Anastasiou D, Takeuchi K, Kahoud ER, Haviv S, Asara JM, Pandolfi PP, and Cantley LC (2011). Ubiquitination of K-Ras enhances activation and facilitates binding to select downstream effectors. Sci Signal 4, ra13. [PubMed: 21386094]

Shalem O, Sanjana NE, Hartenian E, Shi X, Scott DA, Mikkelson T, Heckl D, Ebert BL, Root DE, Doench JG, et al. (2014). Genome-scale CRISPR-Cas9 knockout screening in human cells. Science 343, 84–87. [PubMed: 24336571]

Treacy-Abarca S, and Mukherjee S (2015). Legionella suppresses the host unfolded protein response via multiple mechanisms. Nat Commun 6, 7887. [PubMed: 26219498]

Udeshi ND, Mertins P, Svinkina T, and Carr SA (2013). Large-scale identification of ubiquitination sites by mass spectrometry. Nat Protoc 8, 1950–1960. [PubMed: 24051958]

Verstreken P, Ohyama T, Haueter C, Habets RL, Lin YQ, Swan LE, Ly CV, Venken KJ, De Camilli P, and Bellen HJ (2009). Tweek, an evolutionarily conserved protein, is required for synaptic vesicle recycling. Neuron 63, 203–215. [PubMed: 19640479]

Wang T, Wei JJ, Sabatini DM, and Lander ES (2014). Genetic screens in human cells using the CRISPR-Cas9 system. Science 343, 80–84. [PubMed: 24336569]

Weber SS, Ragaz C, Reus K, Nyfeler Y, and Hilbi H (2006). Legionella pneumophila exploits PI(4)P to anchor secreted effector proteins to the replicative vacuole. PLoS Pathog 2, e46. [PubMed: 16710455]

Wixler V, Wixler L, Altenfeld A, Ludwig S, Goody RS, and Itzen A (2011). Identification and characterisation of novel Mss4-binding Rab GTPases. Biol Chem 392, 239–248. [PubMed: 21194374]

Zhang Q, Cox D, Tseng CC, Donaldson JG, and Greenberg S (1998). A requirement for ARF6 in Fcgamma receptor-mediated phagocytosis in macrophages. J Biol Chem 273, 19977–19981. [PubMed: 9685333]

Zhou Y, Zhu S, Cai C, Yuan P, Li C, Huang Y, and Wei W (2014). High-throughput screening of a CRISPR/Cas9 library for functional genomics in human cells. Nature 509, 487–491. [PubMed: 24717434]

Highlights:

- CRISPR screen reveals host genes regulating distinct steps of *L. pneumophila* infection

- Previously uncharacterized genes *C1ORF43* and *KIAA1109* regulate phagocytosis

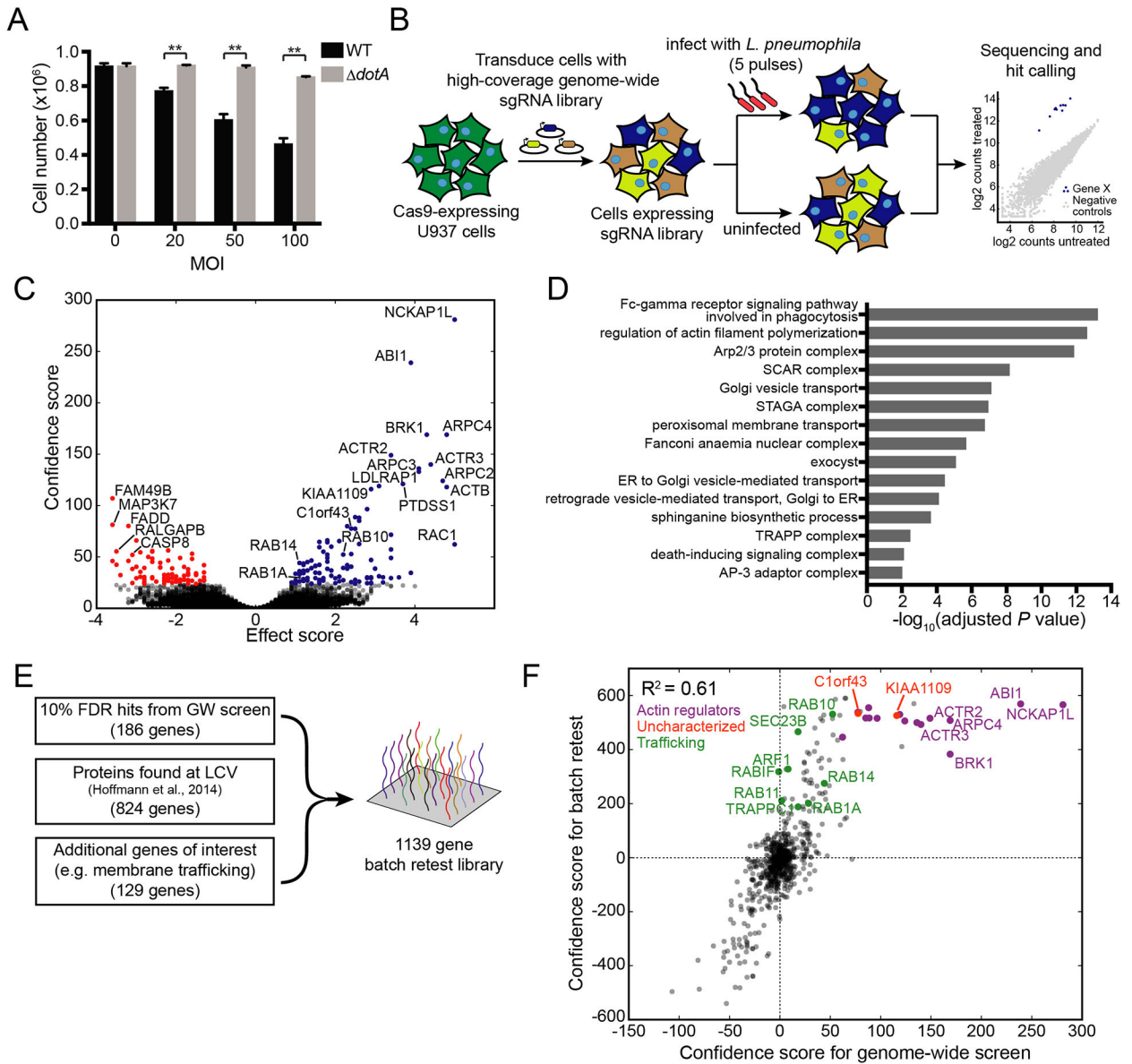- Host Rab10 is hijacked by SidC/SdcA to promote ER recruitment and bacterial replication

Figure 1. CRISPR-Cas9 knockout screens for modifiers of *L. pneumophila* pathogenesis.

(A) U937 cell killing by *L. pneumophila*. U937 cells were infected with the indicated MOI of WT or *dotA L. pneumophila* and live cells were counted 24 hours after infection using flow cytometry and compared between strains (*n* = 2 technical replicates, two-tailed Student's *t* test, **P<0.01; error bars, s.d.

(B) Schematic of screen. Cas9-expressing U937 cells were infected with a genome-wide lentiviral sgRNA library. Half of the population was treated with 5 rounds of *L. pneumophila* infection while the other half was maintained in log-phase growth before quantification by deep sequencing.

(C) Volcano plot of confidence score vs. effect size for all genes. Blue dots indicate genes whose knockout protect host cells from *L. pneumophila* infection and red dots indicate genes whose knockout sensitize host cells to *L. pneumophila* infection using a 10% FDR cutoff. Genome-wide screen results are in Table S1.

(D) Adjusted *P* values for select non-redundant enriched gene-ontology (GO) terms using GOrilla on a ranked list of genome-wide screen hits.

(E) Schematic of genes included in batch retest library. Genes in batch retest library are listed in Table S2.

(F) Correlation of signed confidence scores between genome-wide and batch retest screens. See also Figure S1.
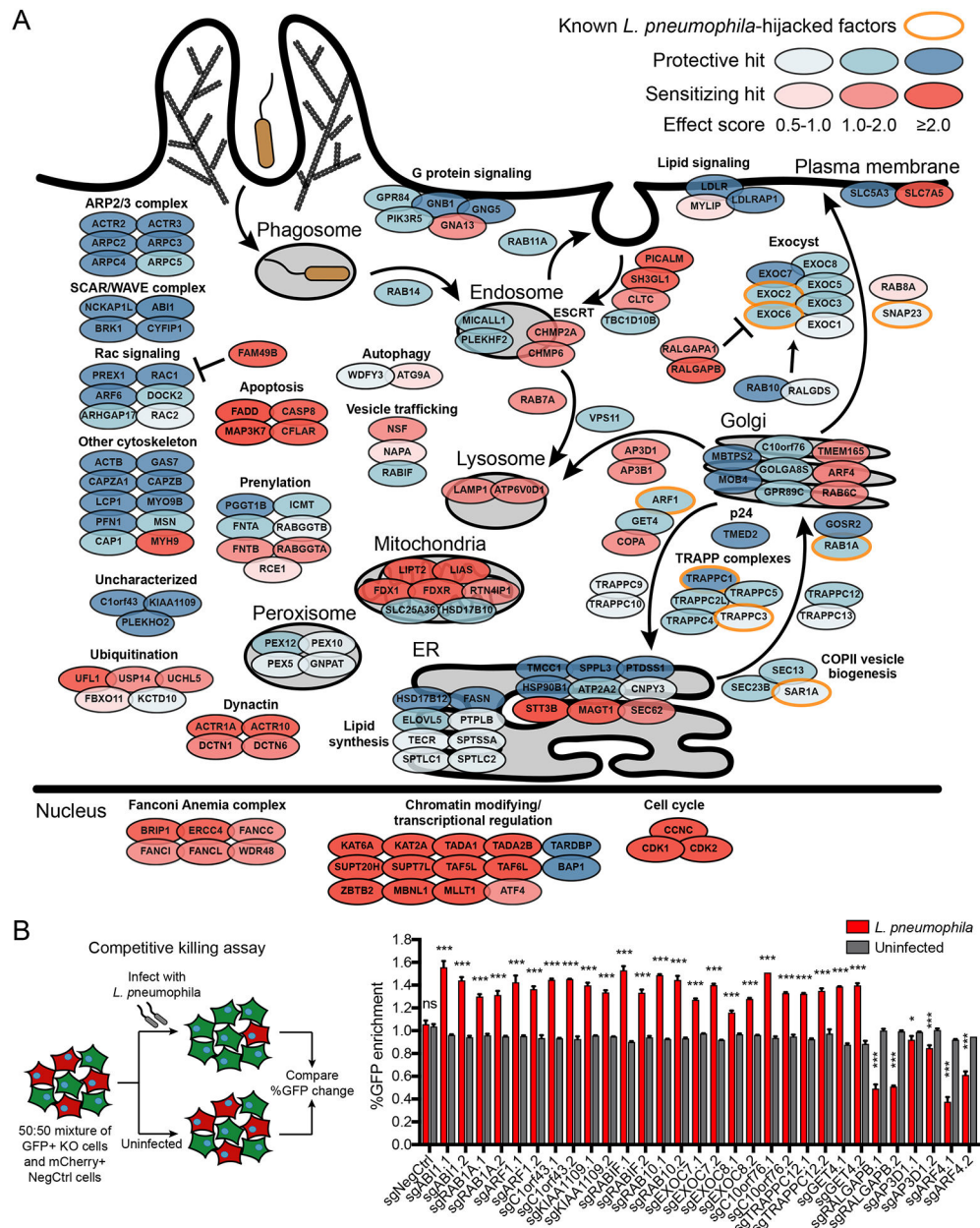
Figure 2. Summary of modifiers of *L. pneumophila* pathogenesis from CRISPR screens

(A) Schematic of selected hits in cellular compartments or processes. Genes are color-coded by effect size. Previously known host factors hijacked by *L. pneumophila* are outlined in orange. Complete batch retest screen results are in Table S3.

(B) Validation of selected hits using individual sgRNAs in a competitive killing assay. Knockout or negative control cells (GFP+) were cocultured with negative control cells (mCherry+) in equal numbers and either infected with *L. pneumophila* at MOI = 100 or left uninfected. The percentage of GFP+ cells was measured by Incucyte and the % GFP change at 48 h was compared between *L. pneumophila*-infected and uninfected populations (*n* = 3 technical replicates, two-tailed Student's *t* test, ns = not significant, *P<0.05, ***P<0.001; error bars, s.d.). Data shown are representative of 2 independent experiments.
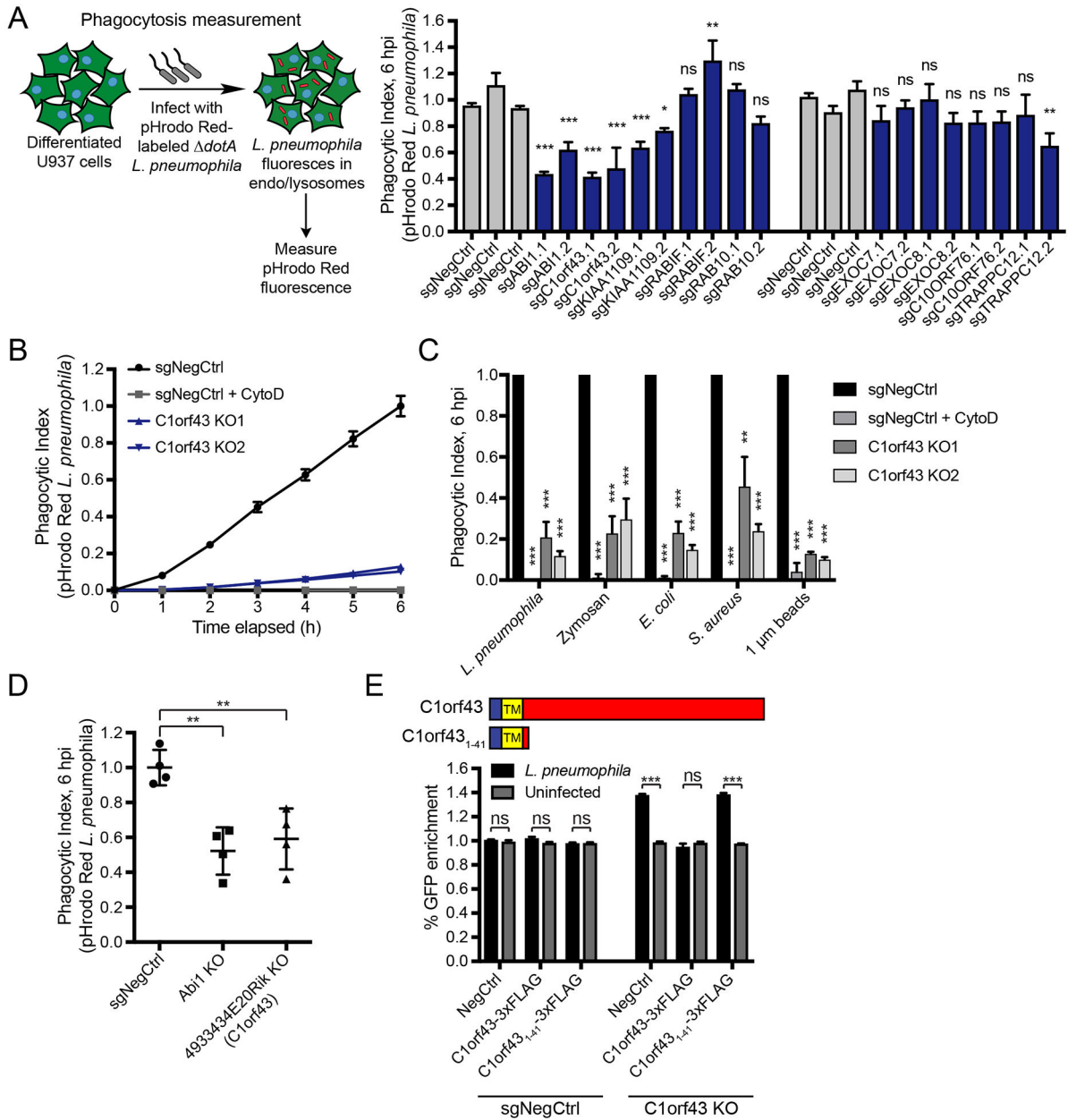
See also Figure S2.

Figure 3. *C1orf43* and *KIAA1109* are regulators of phagocytosis

(A) Effect of gene knockouts on phagocytosis. Differentiated U937 knockout cells (GFP+) were treated with pHrodo Red-labeled ΔdotA *L. pneumophila* at MOI = 10. Phagocytic index was measured as total mCherry fluorescence intensity at 6 h normalized to the number of GFP+ cells. Knockout cells were compared to three negative controls with the most stringent significance value reported (*n* = 4 technical replicates, one-way ANOVA, Dunnett's multiple comparison test, ns = not significant, *P<0.05, **P<0.01, ***P<0.001; error bars, s.d.). Data shown are representative of 3 independent experiments.

(B) Timecourse measurements of pHrodo Red-labeled ΔdotA *L. pneumophila* phagocytosis for *C1orf43* clonal knockout cells. Negative control cells treated with 5 μg/mL Cytochalasin

D were used as a non-phagocytic control. Data represent mean ± s.d. of 4 technical replicates and are representative of 3 independent experiments.

(C) Phagocytosis of various prey particles in *C1orf43* clonal knockout cells. U937 *C1orf43* knockout clones or negative control cells were treated with pHrodo Red-labeled *dotA L. pneumophila*, *E. coli*, *S. aureus*, zymosan, and 1 μm amino magnetic polystyrene beads and phagocytic index was measured at 6 h. Negative control cells treated with 5 μg/mL Cytochalasin D were used as a non-phagocytic control. Cytochalasin D-treated and *C1orf43* knockout cells were compared to WT cells ($n = 3$ independent experiments, two-tailed Student's *t* test, **P<0.01, ***P<0.001; error bars, s.d.

(D) Phagocytosis of *L. pneumophila* in Raw 264.7 mouse macrophages. Raw 264.7 cells were treated with pHrodo Red-labeled *dotA L. pneumophila* and phagocytic index was measured at 6 h. Data represent mean ± s.d. of 4 individual knockout clones for each gene, with each clone used to perform the experiment in technical quadruplicates. Knockout cells were compared to negative control cells ($n = 4$ individual knockout clones, two-tailed Student's *t* test, **P<0.01

(E) Overexpression of C1orf43 rescues *C1orf43* knockout phenotype in a competitive killing assay. GFP+ U937 *C1orf43* clonal knockout cells or negative control cells were lentivirally infected with constructs encoding C-terminal 3xFLAG-tagged full-length C1orf43 or the first 41 amino acids of C1orf43 (C1orf43$_{1-41}$), or a negative control (GFP). These cells were cocultured with mCherry+ negative control cells in equal numbers and infected with *L. pneumophila* at MOI = 100 or left uninfected. The percentage of GFP+ cells was measured by Incucyte and the % GFP change at 24 h was calculated. *L. pneumophila*-infected cells were compared to uninfected cells ($n = 3$ technical replicates, two-tailed Student's *t* test with Holm-Sidak multiple comparisons correction, ns = not significant, ***P<0.001; error bars, s.d.). Data shown are representative of 2 independent experiments. Cartoon shows C1orf43 domain structure and C1orf43$_{1-41}$ truncation mutant. TM indicates the single-pass transmembrane domain in C1orf43.
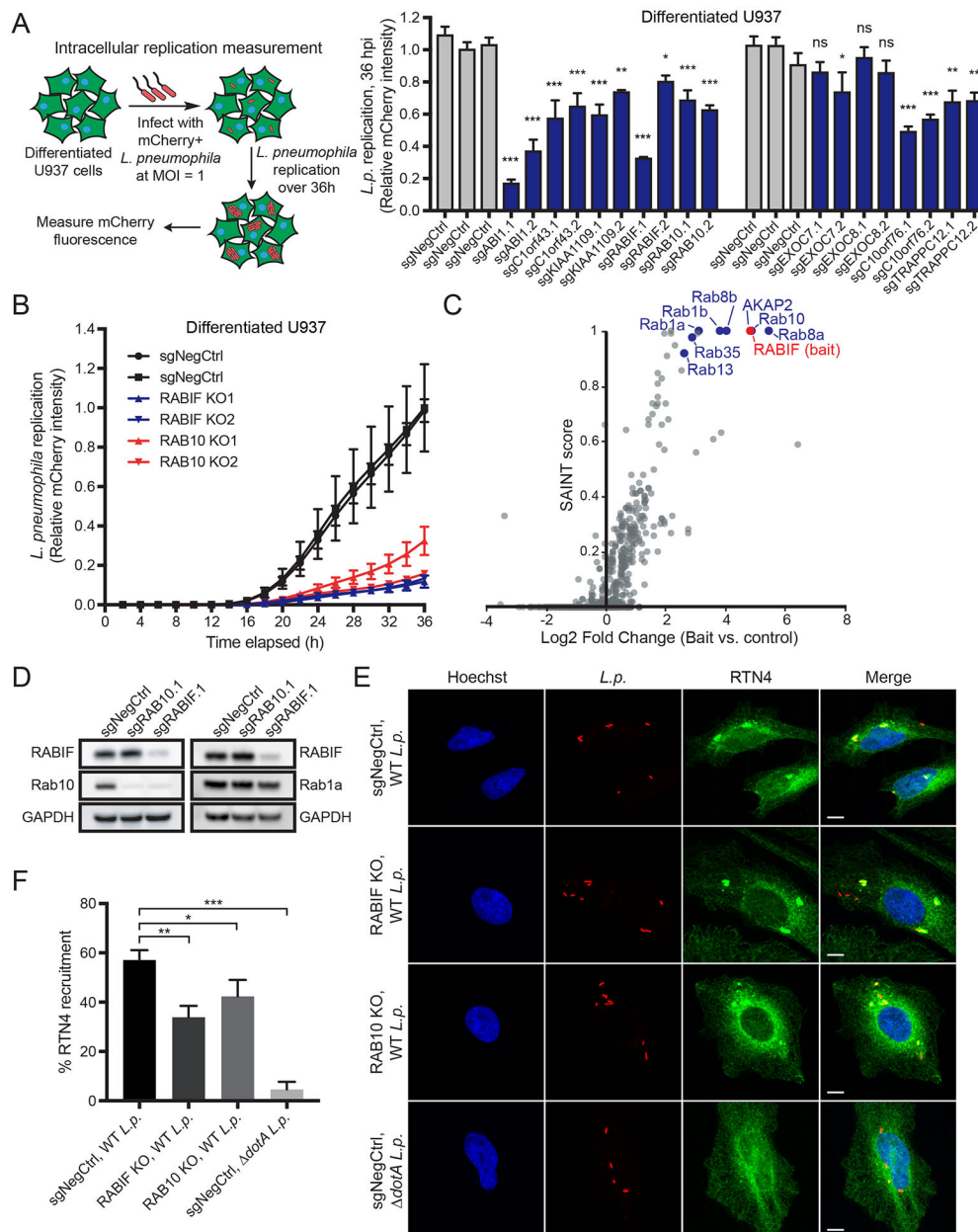
See also Figure S3.

Figure 4. RABIF regulates _L. pneumophila_ replication and ER recruitment to the LCV by stabilizing Rab10 expression

(A) Effect of gene knockouts on _L. pneumophila_ burden. Differentiated U937 knockout cells were infected with mCherry-expressing _L. pneumophila_ at MOI = 1. Total mCherry fluorescence intensity per well was measured by Incucyte at 36 h as a combined metric of _L. pneumophila_ uptake and intracellular replication. Knockout cells were compared to three negative controls with the most stringent significance value reported ($n = 3$ technical replicates, one-way ANOVA, Dunnett's multiple comparison test, *P<0.05, **P<0.01, ***P<0.001; error bars, s.d.). Data shown are representative of 2 independent experiments. (B) _L. pneumophila_ intracellular replication analysis in _RABIF_ and _RAB10_ clonal knockout cells. Differentiated U937 clonal knockout cells were infected with mCherry-expressing _L._

pneumophila at MOI = 1. Total mCherry fluorescence intensity was measured by Incucyte every 2 h for 36 h and compared between knockout cells and negative control cells. Data represent mean ± s.d. of 3 technical replicates and are representative of 2 independent experiments.

(C) Results from GFP-RABIF affinity purification followed by mass spectrometry (APMS). U937 cells stably expressing GFP-RABIF or GFP (negative control) were lysed and co-immunoprecipitated using anti-GFP beads. Each data point represents a protein identified by mass spectrometry. The x-axis shows $\log_2$ fold enrichment of the protein in the GFP-RABIF pull-down vs. GFP pull-down using the geometric mean of three experimental replicates. The y-axis shows the confidence score (SAINT score). Tabular AP-MS results are in Table S4.

(D) Immunoblot analysis of RABIF, Rab10, and Rab1a levels in U937 RABIF and RAB10 knockout cells or negative control cells.

(E) HeLa Fcγ RII *RABIF* and *RAB10* clonal knockout cells or negative control cells were infected with WT or *dotA L. pneumophila* (*L.p.*) at MOI = 1 for 4 h, fixed, and immunostained for *L. pneumophila* (red) and RTN4 (green). Nuclei were stained with Hoechst dye (blue). Scale bar, 10 μm.

(F) Quantification of the percentage of individual intracellular *L. pneumophila* co-localizing with RTN4. Knockout cells were compared to negative control cells for infection with WT *L. pneumophila* (*n* = 3 technical replicates with at least 50 LCVs analyzed per replicate, two-tailed Student's *t* test, *P<0.05, **P<0.01, ***P<0.001; error bars, s.d.
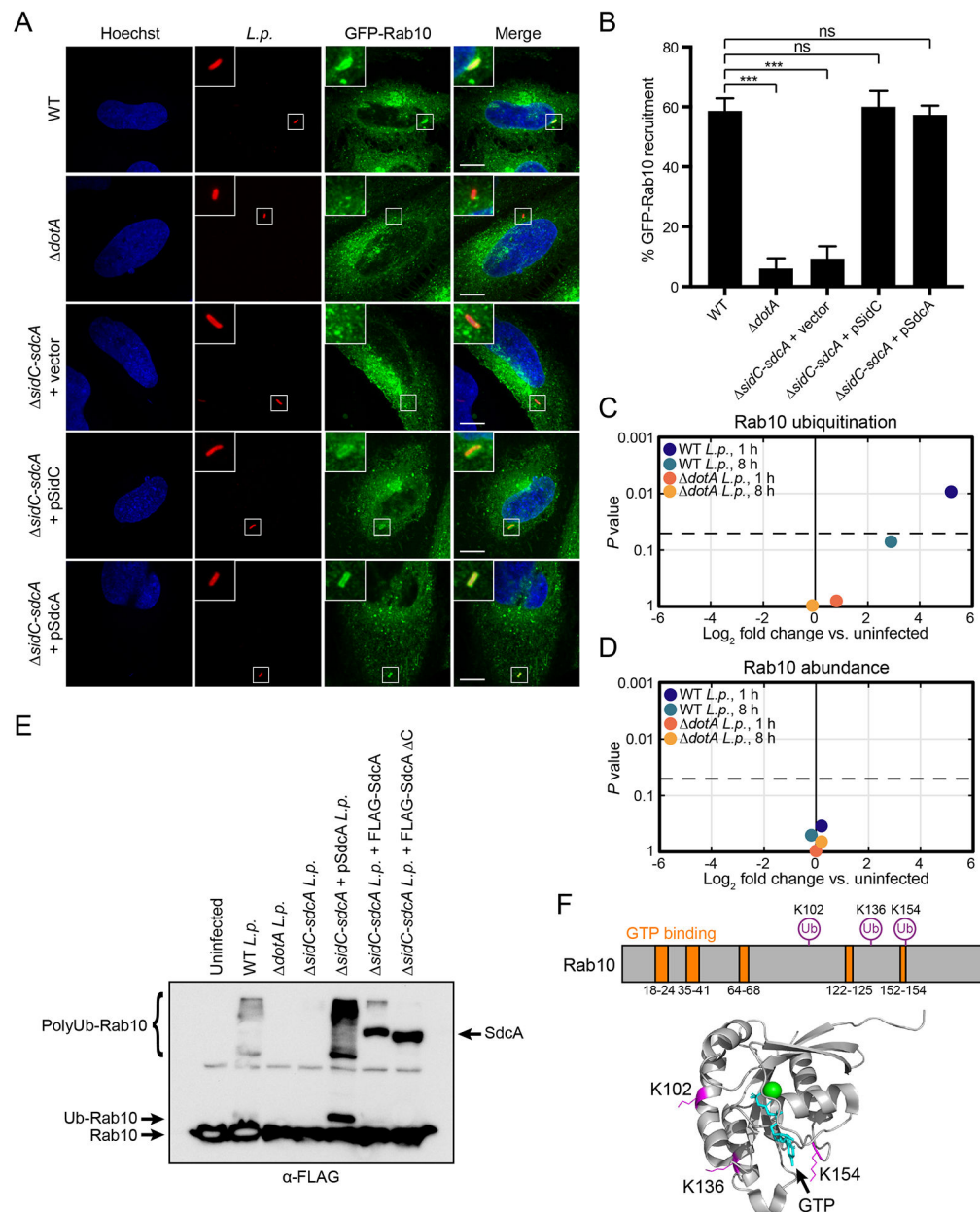
See also Figures S4 and S5.

Figure 5. Rab10 is recruited to the LCV and ubiquitinated by SidC/SdcA during *L. pneumophila* infection

(A) HeLa FcγRII cells stably expressing GFP-Rab10 were infected with WT, ΔdotA, or ΔsidC-sdcA complemented with empty vector, or plasmid-encoded SidC or SdcA *L. pneumophila* at MOI = 3 for 1 h, fixed, and immunostained for *L. pneumophila* (red). Nuclei were stained with Hoechst dye (blue). Scale bars, 10 μm.

(B) Quantification of the percentage of intracellular *L. pneumophila* co-localizing with GFP-Rab10 for the indicated *L. pneumophila* strains. Mutant *L. pneumophila* strains were compared to WT *L. pneumophila* (*n* = 3 technical replicates with at least 50 LCVs analyzed per replicate, two-tailed Student's *t* test, ns = not significant, ***P<0.001; error bars, s.d.

(C and D) HEK293 FcγRII cells were infected with WT or *dotA L. pneumophila* at MOI = 100 for 1 h or 8 h and Rab10 ubiquitination (C) and protein abundance (D) were analyzed by mass spectrometry ($n = 3$ biological replicates). Plots show $\log_2$ fold change vs. uninfected control (x-axis) vs. *P* value (y-axis). Dotted line represents *p*-value cutoff of 0.05.

(E) Immunoblot analysis of Rab10 ubiquitination. HEK293 FcγRII cells stably expressing 3xFLAG-Rab10 were either untransfected (lanes 1–5) or transfected with FLAG-tagged full-length SdcA or SdcA lacking residues 222–315 (lanes 6 and 7); 21 h after transfection, cells were either uninfected or infected with WT, *dotA*, *sidC-sdcA*, or *sidC-sdcA* complemented with plasmid-encoded SdcA *L. pneumophila*. Cells were lysed 1 h post-infection and probed with anti-FLAG antibody.

(F) Schematic and 3D structure showing Rab10 residues ubiquitinated by *L. pneumophila* during infection. Green, Mg^{2+}; Teal, GTP; Magenta, ubiquitinated residues.

See also Figure S5.

KEY RESOURCES TABLE

REAGENT or RESOURCE	SOURCE	IDENTIFIER
Antibodies		
Rabbit polyclonal anti-Legionella	Thermo Fisher Scientific	Cat#PA1–7227; RRID: AB_559903
Mouse polyclonal anti-Legionella	Arasaki and Roy, 2010	N/A
Rabbit polyclonal anti-Nogo A+B	Abcam	Cat#ab47085; RRID: AB_881718
Mouse monoclonal anti-Cytochrome C	BD	Cat#556432; RRID: AB_396416
Mouse monoclonal anti-GM130	BD	Cat#610822; RRID: AB_398141
Mouse monoclonal anti-LAMP1 (D4O1S)	Cell Signaling Technology	Cat#15665; RRID: AB_2798750
Rabbit monoclonal anti-FLAG (D6W5B)	Cell Signaling Technology	Cat#14793; RRID: AB_2572291
Mouse monoclonal anti-FLAG M2	Sigma-Aldrich	Cat#F1804; RRID: AB_262044
Mouse monoclonal anti-RABIF (D-12)	Santa Cruz Biotechnology	Cat#sc-390759; RRID: AB_2756826
Rabbit monoclonal anti-Rab10 (D36C4)	Cell Signaling Technology	Cat#8127; RRID: AB_10828219
Rabbit polyclonal anti-Rab1A (C-19)	Santa Cruz Biotechnology	Cat#sc-311; RRID: AB_632290
Mouse monoclonal anti-GAPDH (6C5)	Thermo Fisher Scientific	Cat#AM4300; RRID: AB_2536381
Bacterial and Virus Strains		
Legionella pneumophila serogroup 1 strain Lp01	Berger and Isberg, 2003	N/A
Lp01 *dotA*	Berger and Isberg, 2003	N/A
Lp01 mCherry	Laboratory of Craig Roy	N/A
Lp01 *SidC-SdcA* + vector	Laboratory of Craig Roy	N/A
Lp01 *SidC-SdcA* + pSidC	Laboratory of Craig Roy	N/A
Lp01 *SidC-SdcA* + pSdcA	Laboratory of Craig Roy	N/A
Legionella pneumophila serogroup 1 strain Lp02 *rpsL hsdR thyA-*	Berger and Isberg, 2003	N/A
Lp02 *dotA*	Berger and Isberg, 2003	N/A
Lp02 2,3,4,6,7	O'Connor et al., 2011	N/A
Lp02 2,3,6,7	O'Connor et al., 2011	N/A
Lp02 2,3,6	O'Connor et al., 2011	N/A
Lp02 7	O'Connor et al., 2011	N/A
Biological Samples		
Chemicals, Peptides, and Recombinant Proteins		
Rifampicin	Sigma	R3501
pHrodo Red, succinimidyl ester	Thermo Fisher Scientific	P36600
pHrodo Red *E. coli* BioParticles Conjugate for Phagocytosis	Thermo Fisher Scientific	P35361
pHrodo Red *S. aureus* BioParticles Conjugate for Phagocytosis	Thermo Fisher Scientific	A10010
Zymosan A from *Saccharomyces cerevisiae*	Sigma	Z4250
1 µm amino magnetic polystyrene beads	Spherotech	AM-10–10

REAGENT or RESOURCE	SOURCE	IDENTIFIER
Cytochalasin D	Thermo Fisher Scientific	PHZ1063
Isopropyl β-D-thiogalactoside	Sigma	I6758
Hoechst 33342	Thermo Fisher Scientific	H3570
Brefeldin A	LC Laboratories	B-8500
Nocodazole	Sigma	M1404
GFP-Trap_A	Chromotek	Gta-20
Janelia Fluor 646 HaloTag ligand	Laboratory of Luke Lavis	N/A
Critical Commercial Assays		
Deposited Data		
Raw sequencing data from screens	This paper	SRA: SRP202048
Experimental Models: Cell Lines		
Human: U937 cells	ATCC	CRL-1593.2
Human: HeLa cells	ATCC	CCL-2
Human: HEK293 cells	ATCC	CRL-1573
Mouse: Raw 264.7 cells	ATCC	TIB-71
Experimental Models: Organisms/Strains		
Oligonucleotides		
See Table S5 for sgRNAs used	This paper	N/A
Recombinant DNA		
LentiCas9-Blast	Sanjana et al., 2014	Addgene Plasmid #52962
pHR-UCOE-EF1A-Cas9-BFP	Jonathan Weissman	N/A
pMCB306 (pSico-pU6-sgRNA EF1A-Puro-T2A-GFP)	Deans et al., 2016	Addgene Plasmid #89360
pMCB320 (pSico-pU6-sgRNA EF1A-Puro-T2A-mCherry)	Morgens et al., 2017	Addgene Plasmid #89359
pSico-EF1A-Puro-T2A-C1ORF43-GFP	This paper	N/A
pSico-EF1A-G418-T2A-C1ORF43–3xFLAG	This paper	N/A
pSico-EF1A-G418-T2A-C1ORF43$_{1-41}$-3xFLAG	This paper	N/A
pSico-EF1A-Puro-T2A-GFP-RABIF	This paper	N/A
pSico-EF1A-Puro-T2A-GFP-RAB10	This paper	N/A
pSico-EF1A-Puro-T2A-GFP-RAB10 Q68L	This paper	N/A

REAGENT or RESOURCE	SOURCE	IDENTIFIER
pSico-EF1A-Puro-T2A-GFP-RAB10 T23N	This paper	N/A
pSico-EF1A-Puro-T2A-GFP-RAB10 K154A	This paper	N/A
pCDNA4/T0-FLAG-SdcA	Horenkamp et al., 2014	N/A
pCDNA4/T0-FLAG-SdcA C	Horenkamp et al., 2014	N/A
Software and Algorithms		
casTLE	Morgens et al., 2017	https://bitbucket.org/dmorgens/castle
GOrilla	Eden et al., 2009	http://cbl-gorilla.cs.technion.ac.il/
SAINT	Choi et al., 2011	https://reprint-apms.org/
MaxQuant	Cox and Mann, 2008	https://maxquant.org/
MSstats	Choi et al., 2014	https://bioconductor.org/packages/release/bioc/html/MSstats.html
Fiji	Schindelin et al., 2012	https://fiji.sc/
Prism	Graphpad	https://www.graphpad.com/
Cytoscape	Shannon et al., 2003	https://cytoscape.org/
PyMOL, Version 2.0	Schrödinger	https://pymol.org/2/
Other		